Optogenetic Characterization of the Stress-associated Focal Adhesion to Cluster Transition of Profilin-VASP Biomolecular Condensates

By

Jahiem Terrell Hill

July, 2025

Director of Thesis: Robert M. Hughes, Ph.D.

Department of Chemistry

ABSTRACT

OptoProfilin, a light-sensitive biosensor derived from Arabidopsis thaliana Cryptochrome 2, triggers profilin oligomerization when exposed to blue light. The primary objectives of this study are to investigate the biochemical composition of stress-associated clusters formed with OptoProfilin and to investigate individual amino acid residues within OptoProfilin and its VASP binding partner to determine their role in its response to light activation. Ultimately, this work seeks to understand the binding proteins and cell stress pathways involving profilin and VASP that contribute to stress granule formation and biomolecular structures. The observed OptoProfilin response to energetic and oxidative stress may offer valuable information about diseases in which profilin has been implicated as a key component of disease progression. Our findings identify mutations that have significant effects on the OptoProfilin response, including the identification of a new knockout mutant of OptoProfilin activity. We have also identified focal-adhesion associated proteins (zyxin, vinculin, paxillin) that are co-localized in OptoProfilin

in focal adhesion (zyxin, vinculin, paxillin) and in stress-associated clusters (zyxin, vinculin). This result supports our general hypothesis of a multi-layered model of focal adhesion composition.

Optogenetic Characterization of the Stress-associated Focal Adhesion to Cluster Transition of Profilin-VASP Biomolecular Condensates

A Thesis

Presented to the Faculty of the Department of Chemistry

East Carolina University

In Partial Fulfillment of the Requirements for the Degree

Master of Science in Chemistry

By

Jahiem Terrell Hill

July, 2025

Director of Thesis: Robert Hughes, Ph.D.

Thesis Committee Members:

Erzsebet Szatmari, Ph.D.

Colin Burns, Ph.D.

Eli Hvastkovs, Ph.D.

ACKNOWLEDGEMENTS

This journey would not have been possible without the tremendous support of the Golden Leaf Foundation, which supported my academic foundation. I wish to express my deepest appreciation to my mother, Harriet Flowers, for her unconditional love and support. There was a time in my life I didn't think you would make it to see me achieve graduating not once but twice surpassing your educational attainment level so this one's for you.

I was blessed to have an amazing mentor, Dr. Robert Hughes, for his dedication, guidance, and wisdom throughout my endeavors. I will never forget the many 8am lab meetings, bad movie talks, and serious life advice you have given me.

Furthermore, I extend my gratitude to my close friends, family, and the faculty of the ECU Department of Chemistry, whose encouragement has been instrumental in recognizing my potential within the scientific community and motivating me to pursue future endeavors. Thank you.

It would be remiss of me not to acknowledge Harris Bruce Flowers, my grandfather. His passing from ALS ignited my desire to contribute to the scientific community and pursue my education further. He remains the inspiration for this journey of giving back to the world of science, medicine, and community.

TABLE OF CONTENTS

LIST OF TABLES

LIST OF FIGURES

CHAPTER 1

OptoProfilin: Single Component Biosensor of Applied Stress

(Reproduced in part with permission from Mann, N., Hill, J., Wang, K., Hughes, R. M. (2024). Chem. Biochem. e202400007.)

1.1 Introduction

Profilin is recognized as a crucial target for a wide range of diseases and abnormal cytoskeletal dynamics due to its significant role in actin filament elongation, cell migration, and various nucleation factors (Lee et al., 2024). Previous research has also demonstrated that profilin is linked to both cofilin−actin rod formation (Munsie and Truant, 2012; Walter et al., 2021) and stress granule assembly (Figley et al., 2014), thus connecting profilin to diseases characterized by aberrant cytoskeletal dynamics, including cancer (Mahboubi and Stochaj, 2017), cardiovascular disease (Wang et al., 2022), and neurodegenerative disease (Borovac et al., 2018; Wurz et al., 2022b; Read et al., 2023). Precise control of profilin's biochemical activity would be advantageous to our understanding of its role in aberrant cytoskeletal dynamics and human disease. Optogenetics enables precise control of a protein's biochemical activity with light. The rise of optogenetics has shown exciting potential in modulating cellular functions through membrane-less assemblies and being incorporated into biosensors for early disease detection (Lee et al., 2024). By using an optogenetic strategy to control profilin activity it is possible to control this key regulator of actin dynamics and probe its role in disease associated cytoskeletal dysregulation (Lee et al., 2024).

In our laboratory, we previously developed the CofActor optogenetic system, which utilizes cofilin and actin as a light-regulated biosensor of cofilin actin rod formation. In the CofActor system, the interaction of these two proteins results in a light- and stress-gated clustering response (Salem, Bunner et. al. 2021). In this initial work, a limited characterization of the actin

ATP binding site was performed to better define the contributions of nucleotide binding residues under both stress- and non-stress conditions to cytoskeletal anomalies. It was discovered that mutagenesis of actin S14 leads to rods, clumps, or condensates under different experimental conditions than the wild-type actin used in the initial CofActor system. This result also invited further investigation into the composition of the CofActor system, including whether substituting an actin-binding protein other than cofilin into the CofActor framework would have an effect on its ability to detect cellular stress. As a result of this line of inquiry, OptoProfilin was created and found to act as a stand-alone biosensor of cellular stress and, under conditions of homeostasis, a unique light-responsive locator of focal adhesions in adherent cells (Mann et al., 2024).

The specific mechanisms by which OptoProfilin promotes the stress-associated formation of biomolecular condensates remains unclear. This presents a significant challenge in studying these complex interactions due to the many unknown components involved. In this thesis, I have selected and investigated amino acid residues in within OptoProfilin and its binding partner VASP that may be critical for their light- and stress-gated interaction. In addition, I have performed experiments to investigate whether cytoskeleton-associated proteins other than profilin and VASP are present within OptoProfilin-associated clusters and focal adhesion. In the course of these work, I have identified unique mutants that promote unique responses of the OptoProfilin reagent, including knockout and dominant negative mutants. In addition, we have demonstrated varying responses among the focal adhesion-associated proteins zyxin, vinculin, and paxillin to OptoProfilin-mediated cluster formation.

1.2 Profilin

Profilin is a 15 (kDa) actin-monomer-binding protein that is responsible for dual function depending on the capping of barbed ends. When barbed ends are blocked by capping proteins,

profilin sequesters G-actin (Gutsche-Perelroizen et al., 1999). In contrast, in motile regions of the cell where uncapped barbed ends are actively elongated, the profilin-actin complex can actively participate in filament growth (Pollard and Cooper, 1984; Pantaloni and Carlier, 1993). This is done in a 1:1 equimolar ratio and the dynamics of this is well studied in the context of cell motility and mechanics (Blanchoin et al., 2014). Little is known about the associated proteins properties that profilin has on their cellular dynamics under different conditions. Additionally, as a mediator of Arp 2/3 actin filament branching profilin can be linked to stress granule assembly involved in a range of aberrant cytoskeletal dynamics including cancer (Mahboubi and Stochaj, 2017), cardiovascular disease (Wang et al., 2022), and neurodegenerative disease (Borovac et al., 2018; Wurz et al., 2022b; Read et al., 2023).

Different isoforms of profilin are found in non-neuronal cells and other non-muscular cells, for example, Gau et. al., 2019 found that Profilin 1 is critical for efficient cell migration in breast cancer cells. In addition, cell-to-substrate adhesion promoted the interaction between VASP and Profilin 1 through the reduction of PKA activity Gau et al., 2019, which would otherwise phosphorylate Pfn1 (Profilin 1) at Ser137 and hinder its interaction with VASP (Reinhard et al., 1995). The phosphorylation of Pfn1 at this site, driven by the cAMP/PKA pathway, was found to impair cell motility by disrupting the adhesion-protrusion coupling mechanism. A downregulation of PKA-activity increases this profilin 1-VASP effect on migration. Confirmed with site-directed mutagenesis, the phosphorylation of Ser137 of profilin was partially responsible for the anti-migratory effects **(Figure 1.1)**.

Another major finding from this study is the regulation of profilin-1 VASP opened a new possibility of adhesion-protrusion coupling through time-dependent regulation of PKA activity and profilin interaction with formin proteins that could serve as a brake when a new protrusion

has formed preventing profilin VASP interaction (Reinhard et al., 1995). The FH1 domain of Arabidopsis FORMIN1 (AtFH1) is also reported to modulate actin nucleation and polymerization in vitro (Michelot et al., 2005). Recently, two groups reported that profilin functions as a gatekeeper during the construction of different actin networks generated by formin or ARP2/3 complex in yeast and mammalian cells (Rotty et al., 2015; Suarez et al., 2015).

Profilin 2 is a specific isoform primarily found in neurons, although it also appears at lower levels in other structurally similar tissues where it can bind to similar ligands (Mouneimne et al., 2012). While it shares structural resemblances with other isoforms, Profilin 2 exhibits distinct binding affinities for various ligands. Both Profilin 2 and EVL play a critical role in suppressing cellular protrusion and motility, a process that depends on actomyosin contractility. Significantly, a reduction in either EVL or Profilin 2 enhances invasion in both in vitro and in vivo settings (Mouneimne et al., 2012).

Figure 1.1 Profilin impact at position S137 in the phosphorylation pathway. The upregulation of MMP2 and MMP9 is influenced by the phosphorylation of Pfn1 at S137

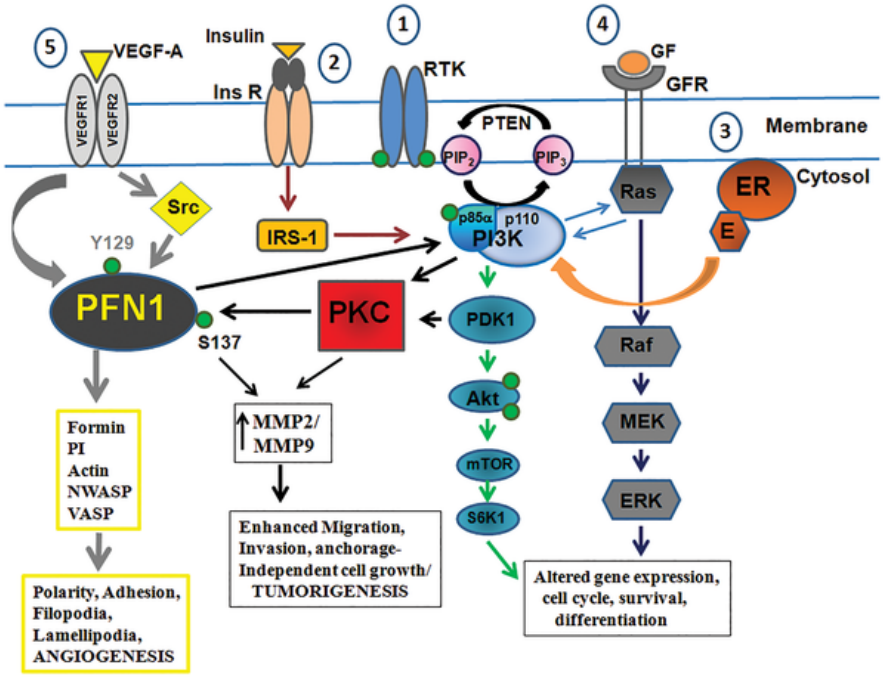

Enhancing migration. PKC is also an influence on this action by activating P13K by association with Profilin. Image used under Creative Commons license: CC BY- 4.0 DEED

Not only does Profilin bind to VASP for cell signaling, but cell plasticity is also shown to be affected by this binding as demonstrated in a study done on fear-conditioned rats (Basu et al., 2016). When the actin scaffolding-associated protein Arp2/3 co-exists with profilin within the lateral amygdala neurons, it was discovered that the interaction between VASP and profilin is crucial for stabilizing the actin cytoskeleton and maintaining the morphology of dendritic spines (Basu et al., 2016).

1.3 VASP

The VASP (Vasodilator-Stimulated Phosphoprotein) homology domain is an important structural feature of this VASP-profilin binding and plays a significant role in cell motility, adhesion, and cytoskeletal dynamics (Ball et al., 2001; Döppler and Storz, 2013) VASP is a member of the Ena/VASP family of proteins and is known for its ability to bind to actin filaments and promote actin polymerization. This function is directly related to the formation of lamellipodia and filopodia, both essential for successful cell migration (Ball et al., 2001; Oldenburg et al., 2015)

The EVH1 domain of VASP is a total of 380 residues containing 3 distinct regions **(Table 2.1)**. The first 115-residue protein-protein interaction module on the VASP domain plays a crucial role in linking their host proteins to various signal transduction pathways (Ball et al., 2001). EVH1 domain also recognizes and binds specific proline-rich sequences (PRSs) with low affinity but high specificity, which allows for profilin to bind and conformationally activate this signaling pathway (Reinhard et al., 1995). The binding mechanism involves a small 'core' PRS that binds a 'recognition pocket' on the domain surface, with further interactions enhancing affinity and

specificity. The proposed structure of EVH1 and associated domains are shown in (**Figure 1.2)** of a nanoscale protein organization (Kanchanawong et al., 2010).

Table 2.1 VASP Amino Acid Sequence and Regions (UniProt, 2024).

VASP Sequence
MSETVICSSRATVMLYDDGNKRWLPAGTGPQAFSRVQIYHNPTANSFRVVGRKMQP DQQVVINCAIVRGVKYNQATPNFHQWRDARQVWGLNFGSKEDAAQFAAGMASALE ALEGGGPPPPPALPTWSVPNGPSPEEVEQQKRQQPGPSEHIERRVSNAGGPPAPPAGGP PPPPGPPPPPGPPPPPGLPPSGVPAAAHGAGGGPPPAPPLPAAQGPGGGGAGAPGLAAA IAGAKLRKVSKQEEASGGPTAPKAESGRSGGGGLMEEMNAMLARRRKATQVGEKTP KDESANQEEPEARVPAQSESVRRPWEKNSTTLPRMKSSSSVTTSETQPCTPSSSDYSDL QRVKQELLEEVKKELQKVKEEIIEAFVQELRKRGSP
EVH1= Red, PPR=Black, EVH2= Blue

According to the Interpro database Wiskott-Aldrich syndrome protein (WASP)-homology domain 2 (EVH2) of human vasodilator-stimulated phosphoprotein and related proteins the classification of this domain is characterized by being small, widespread intrinsically disordered actin-binding peptides displaying sequence variability and different regulations of actin self-assembly in motile and morphogenetic processes. WH2 domains are identified by an actin-binding motif LKKT/V with variable N-terminal and C-terminal extensions.

The last region to discuss is the PPR region that facilitates binding to other proteins and has a high affinity to bind. It is speculated that focal adhesions are formed in a layered approach and VASP is used as a signaling protein that is crucial for lamellipodia and filopodia movement from the literature (Legerstee and Houtsmuller, 2021).

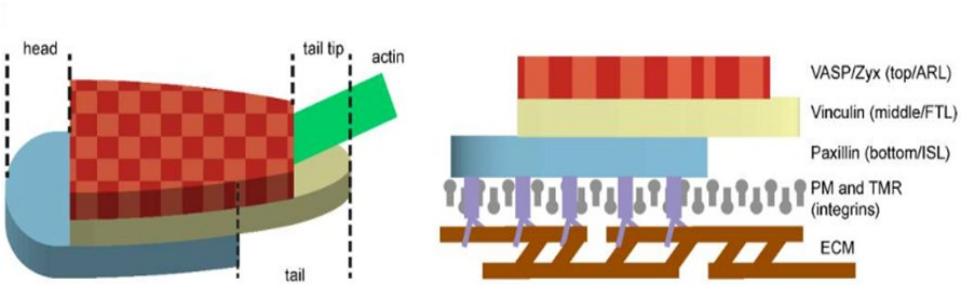

Figure 1.2 Schematic view model of the nanoscale protein organization within focal adhesions Left: Schematic view model of the nanoscale protein organization within focal adhesions**.** Right: Layered approach to focal adhesions (top layer: VASP/Zyxin; middle layer: Vinculin/Talin; bottom layer: Paxillin and FAK). Image used under Creative Commons license: CC BY- 4.0 DEED

When looking at a focal adhesion assembly the top layer of the focal adhesion assembly contains zyxin and VASP. Zyxin, a phosphorylation-dependent adaptor protein, has been shown to play a critical role in regulating the dynamics and structure of these focal adhesion complexes. Specifically, zyxin is recruited to maturing focal adhesions where it binds to and organizes the actin cytoskeleton, stabilizing the adhesion structure (Legerstee and Houtsmuller, 2021; Yoshigi et al., 2005). Additionally, VASP is the other key component of the top layer, also binding to and stabilizing actin filaments within the adhesion complex.

The localization of zyxin and VASP to focal adhesions is dependent on the proper formation and integrity of the underlying integrin-mediated adhesion structure. As the adhesion matures, zyxin and VASP work together to crosslink and bundle actin filaments, reinforcing the linkage between the extracellular matrix and the intracellular cytoskeleton. The dynamics of zyxin and VASP localization to focal adhesions are tightly regulated, and disruptions in this process can impair cell migration, proliferation, and survival (Yoshigi et al., 2005; Legerstee et al., 2019).

Talin and vinculin are central to the middle force transduction layer (FTL) of focal adhesions, which are crucial for cellular adhesion and transduction. In this context, talin and

vinculin both play fundamental roles in linking integrins to the actin cytoskeleton and maintaining the structural integrity of these adhesive sites. Talin binds directly to integrins, facilitating their activation and subsequent attachment to actin filaments. This interaction is critical for focal adhesion assembly and stability.

Conversely, vinculin strengthens these adhesions by connecting talin to the actin network, thus enhancing the mechanical stability of the adhesion sites (Legerstee and Houtsmuller, 2021; Reinhard et al., 1995) The recruitment and activation of these proteins are influenced by cellular forces and signaling cues, making them key players in the regulation of focal adhesion dynamics. Profiling these proteins, alongside other focal adhesion components like VASP, provides insights into their roles in cellular responses to mechanical stress and their contributions to cell movement and function. VASP, known for its involvement in actin filament dynamics and focal adhesion assembly, works in concert with talin and vinculin to modulate cell adhesion and migration (Legerstee et al., 2019).

The bottom integrin signaling layer (ISL) of focal adhesions involves critical proteins such as paxillin and focal adhesion kinase (FAK), which play pivotal roles in signal transduction and cell adhesion. Paxillin is an adaptor protein that is crucial for organizing focal adhesion complexes and transmitting signals from integrins to the intracellular machinery and orientation (Legerstee and Houtsmuller, 2021; Legerstee et al., 2019; Turner, 2000). It interacts with various signaling molecules and cytoskeletal proteins, facilitating the assembly and turnover of focal adhesions. Paxillin's phosphorylation and recruitment are essential for dynamic changes in focal adhesion architecture.

FAK, a non-receptor tyrosine kinase, acts as a central node in integrin-mediated signaling pathways. It is recruited to focal adhesions where it is activated by autophosphorylation and

subsequently phosphorylates various substrates, including paxillin (Legerstee and Houtsmuller, 2021; Hildebrand et al., 1995) This activation cascade promotes cell spreading, migration, and survival by regulating focal adhesion dynamics and cytoskeletal organization. The interplay between FAK and paxillin in the ISL is crucial for translating mechanical and biochemical signals into cellular responses, making these proteins essential to understanding cell adhesion and movement (Kanchanawong et al., 2010).

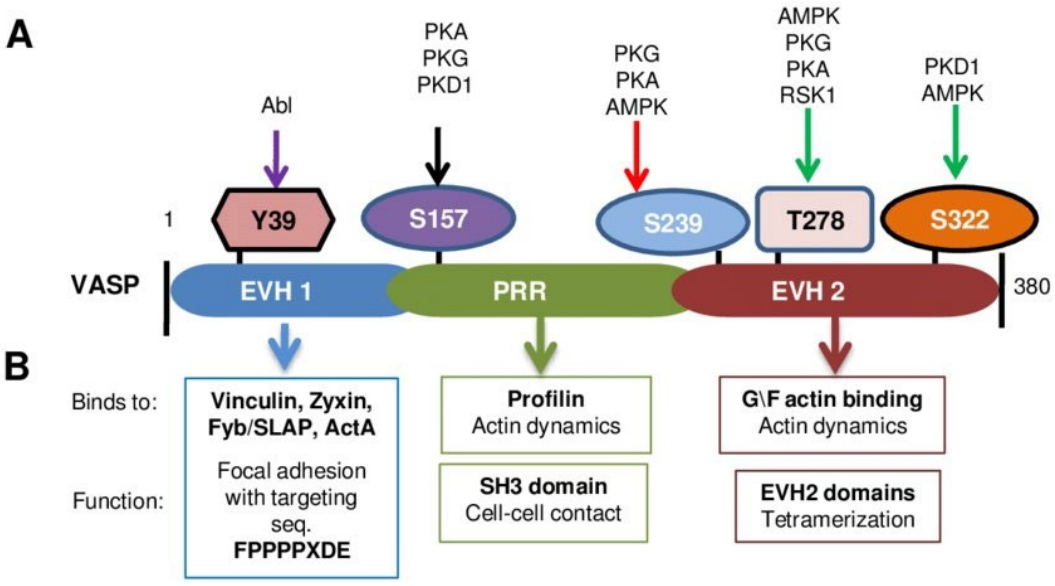

Figure 1.3 Mammalian VASP domain structure
binding partners, phosphorylation sites, and upstream kinases (Döppler and Storz, 2013). Image used under Creative Commons license: CC BY- 4.0 DEED

1.4 Biomolecular Condensates

Cellular stress, particularly osmotic stress, occurs when cells experience significant shifts in their external environment, leading to changes in their internal physical-chemical properties. Environmental fluctuations can cause dramatic alterations in cell volume, intracellular solute concentrations, and macromolecular crowding (Cuevas-Velazquez et al., 2021). Such changes disrupt cellular homeostasis and affect various biomolecular functions. To monitor these rapid intracellular changes, a non-optogenetic biosensor named SED1 (Cuevas-Velazquez et al., 2021),

which uses the Arabidopsis intrinsically disordered AtLEA4-5 protein, leverages the environmental sensitivity of intrinsically disordered protein regions to track osmotic stress in real-time across different species, providing insights into how cells sense and adapt to these stress conditions using fluorescence. SED1 biosensor exhibited significant, near-linear changes in Förster Resonance Energy Transfer (FRET) ratios in response to varying osmolarity levels. This change was dependent on the macromolecular crowding and osmolarity within the cells, showing that the biosensor is sensitive to physical-chemical alterations under stress conditions. The study highlighted that the conformational changes in AtLEA4-5, crucial for the biosensor's function, are sequence-dependent and influenced by environmental conditions, such as macromolecular crowding and the presence of certain osmolytes which can be seen having similar properties to biomolecular condensates.

Biomolecular condensates are micron-scale compartments in eukaryotic cells that lack traditional surrounding membranes yet play crucial roles in cellular organization by concentrating proteins and nucleic acids (**Fig. 1.4)**. These structures are implicated in a variety of essential cellular processes such as RNA metabolism, ribosome biogenesis, DNA damage response, and signal transduction. The formation of biomolecular condensates is primarily driven by liquid-liquid phase separation facilitated by multivalent macromolecular interactions (Banani et al., 2017). This phenomenon provides a physical framework that helps elucidate the mechanisms behind the assembly.

Classic organelles like the endoplasmic reticulum and Golgi apparatus are defined by lipid bilayer membranes that create selective permable barriers, regulating the interior and exterior environments through specialized membrane transport mechanisms. In contrast, many cellular compartments (nucleoli, Cajal bodies, and PML nuclear bodies in the nucleus; stress granules and

germ granules in the cytoplasm) are not bound by membranes (Banani et al., 2017). These structures are characterized by their ability to concentrate proteins and nucleic acids at specific cellular sites without the need for a surrounding barrier.

Recent insights into the biophysical properties of these condensates have been transformative, particularly the understanding that liquid-like properties in C. elegans germ cells, and suggest they form through phase separation from the cytoplasm (Marnik and Updike, 2019). This discovery aligns with observations that many other membrane-less compartments, such as nucleoli and stress granules, also exhibit liquid-like behavior, underscoring phase separation as a widespread mechanism.

Within the actin cytoskeleton network, protein fibers containing actin and other related proteins provide structure to the cell and support for intracellular transport. Focal adhesions are protein complexes, or large macromolecular multiprotein assemblies, which are found along the cell membrane and interact with intracellular protein fibers. Many researchers in the field classify focal adhesions as ‘biomolecular condensates’ because phase separation enables the recruitment of other adhesion proteins (Litschel et al., 2024).

The study of biomolecular condensates extends beyond their formation to encompass their regulation and functional implications. For example, the concentration of reaction components within these compartments can significantly alter reaction kinetics, enhancing specific biochemical pathways while potentially inhibiting activities (Banani et al., 2017). Moreover, the dynamic nature of these condensates allows for rapid assembly and disassembly, enabling cells to swiftly respond to changing physiological conditions. Biomolecular condensates represent a fundamental organizational strategy; their ability to form through phase separation provides a versatile means to regulate biochemical processes, offering new insights into cellular organization and function.

Continued research into the principles governing these structures can promise to deepen our understanding of cellular biochemistry.

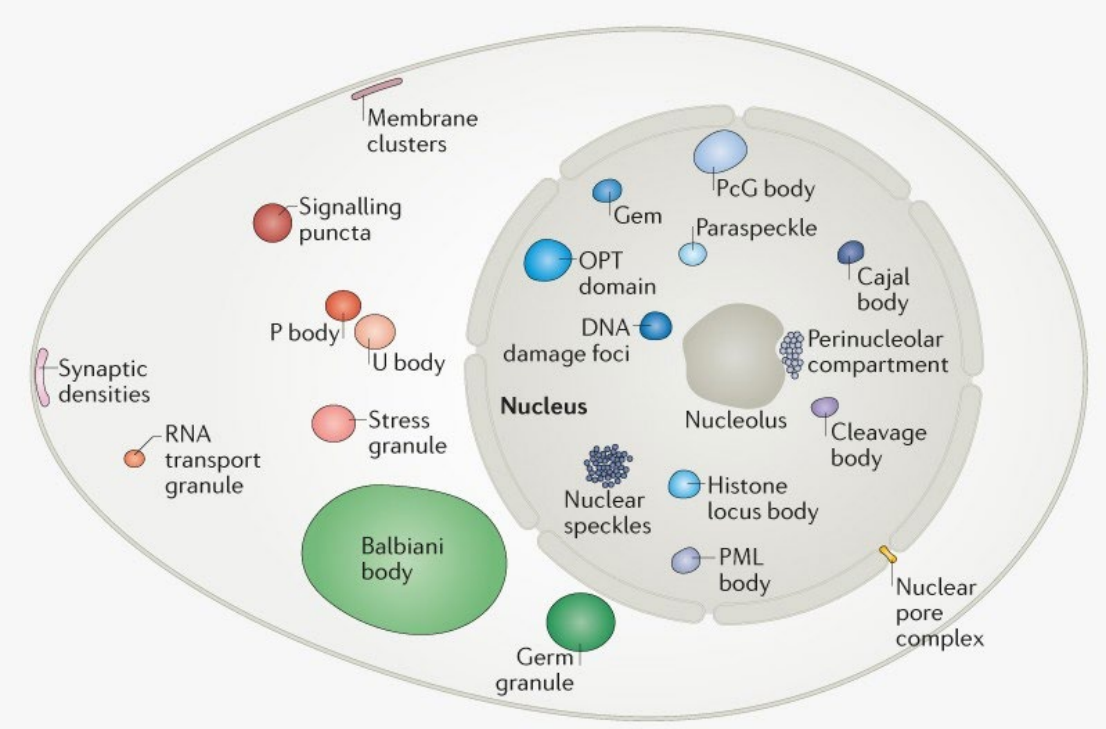

Figure 1.4 Common biomolecular condensates identified. A growing number of biomolecular condensates have been identified in the cytoplasm and nucleus. Not all biomolecular condensates are present in all cell types (Banani et al., 2017). Image used under Creative Commons license: CC BY- 4.0 DEED

1.5 Optogenetics

Optogenetics allows endogenous or engineered photoreceptors to be controlled by light illumination spatially and temporally (Emiliani et al., 2022). One photoreceptor, which contains a chromophore that is bound to an opsin protein, is called rhodopsin. Opsins themselves are membrane bound G protein coupled receptors (GPCRs) that are light gated ion channels that are capable of absorbing light at specific wavelengths. These can be found in Eukaryotic cells and Prokaryotic cells that all involve transfer of energy and bioenergetics. Channelrhodopsins are

derived from the green algae species Chalmydomonas reinhardtii **(Figure 1.5)**. These ion-channels are non-specific in the rhodopsin's Na^+, K^+, Ca^{2+} influxes in and out of the cell membrane (Hososhima et al., 2023). Opposing the channelrhodopsin is the Halorhodopsin that can transport Cl^- in response to yellow light activation and the chromophore that is covalently attaches returns from trans to cis. Optogenetics can also be used to characterize cellular functions that are implicated in the pathologies of various diseases (Bansal et al., 2022). For optogenetics to be applicable in healthcare, characterization of bio-chemical properties is crucial in developing a robust circuit-centric therapeutic that can overcome the limitations of other therapies currently available such as activation and invasiveness. To achieve this, the future of optogenetics focuses on progress toward translational optogenetics, which involves the safe and effective delivery of vectors that allow for spatiotemporally precise interventions that respond to light of an appropriate wavelength and intensity (Bansal et al., 2022). These vectors could reduce or shut down the activity of pathways that are unwanted like cancer or prion formation alternatively they can increase protective pathways.

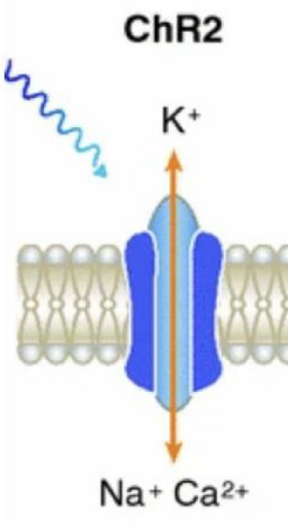

Figure 1.5 Function of the Channelrhodopsin-2. ChR2 is a non-specific cation channel that when activated by blue light, will depolarize, and send cations such as Na^{2+} and Ca^{2+} across the

membrane and into the cell **(**Rein and Deussing, 2012). Image used in accordance with Creative Commons license CC BY-NC 2.0

Alzheimer's Disease (AD) is one of many application examples of how we can use optogenetics to compare different neuronal activities under stressed cells like those of patients with AD and a control. Studies have been done to show an optogenetic-based approach to AD models in *fruit flies, zebrafish, and roundworms* using acute Aβ aggregation (Tiwari and Tolwinski, 2023). These studies shed light on the importance of intracellular aggregates in the progression of AD and the identity of unknown factors that affect its pathology, prompting further investigations such as stress and other co-factors **(Figure 1.6).** More recent research has been tailored to restoration of sight and looking at cardiac functions like wave propagation from impulses to charging a battery pack on a pacemaker through short energy pulses and the use of these optogenetic components.

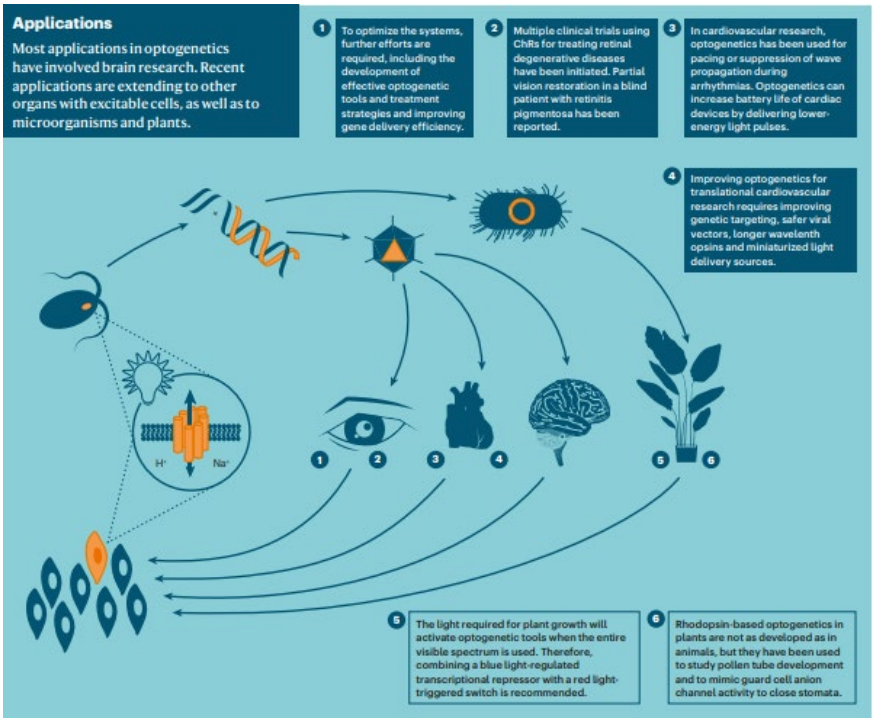

Figure 1.6 Infographic of the expanding applications of optogenetics. (Emiliani et al., 2022). Image used in accordance with Creative Commons license CC BY-NC 2.0

Cryptochrome 2

Central to this research is Cryptochrome 2, also known as CRY2, a flavin adenine dinucleotide-binding protein that is a key component of the circadian core oscillator complex, which regulates the circadian clock (Che et al., 2015). It is an optogenetic target protein that enables precise control over cellular activities through light-induced homo-oligomerization. CRY2 has gained attention due to its ability to respond to blue light, enabling control of various cellular activities. Endogenously, CRY2 undergoes conformational changes upon light absorption, which facilitates interactions with other proteins and influences gene expression (Wurz et al., 2022; Che et al., 2015). The FAD cofactor is a its chromophore which absorbs blue light and allows the FAD to undergo reduction when exposed to the range of 430-490 nm with a lambda max at 450 nm. FAD is reduced by receiving electrons relayed via three evolutionarily conserved tryptophan residues called the 'Trp-triad' (Wang and Lin, 2020). Photoreduced CRY molecules undergo conformational changes to form physiologically active homo-oligomers. Once absorbed by the CRY2 molecules oligomers form spontaneously and dissociate into monomers in 5–10 min by a negative feedback inhibition by the blue-light inhibitors of CRY protein (BIC) in the absence of light (Wang and Lin, 2020). This capability makes CRY2 a powerful tool in optogenetics, where scientists have translated its use as a tool to fuse to a protein of interest to manipulate cellular functions with high temporal and spatial precision in eukaryotic cells. By designing a CRY2 optogenetic tool by using proteins associated with AD such as profilin we can better understand the complexities of AD and develop more effective strategies for intervention and disease models.

OptoProfilin

A Cry2 - Profilin fusion construct ('OptoProfilin') was generated and investigated for its response to either light or a combination of light and energetic stress in HeLa cells **(Figure 1.7).**

Surprisingly, light activation of the profilin construct in the absence of a CIB binding partner induced a subcellular localization response (Mann et al., 2024). To demonstrate that the observed localization pattern was consistent with that of focal adhesions, immunostaining for Paxillin, a focal adhesion localized protein, was performed demonstrating that optically activated OptoProfilin is co-localized with focal adhesions (Mann et al., 2024).

Moreover, the localization of profilin isoforms reveals organ-specific expression patterns. Previous experimental research into a Cry2 - Profilin fusion construct ('OptoProfilin') was generated **(Fig. 1.7)** and investigated for its response to either light or a combination of light and energetic stress in HeLa cells. Surprisingly, light activation of the profilin construct in the absence of a CIB binding partner was sufficient to induce a subcellular localization response with an apparent targeting of focal adhesions.

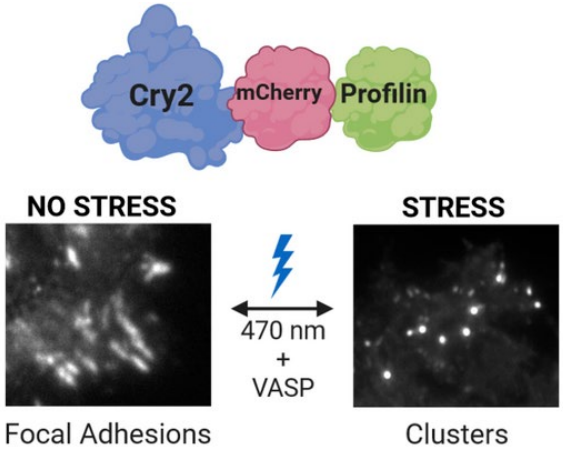

Figure 1.7 Schematic of the OptoProfilin System. Clustering of profilin driven by Cry2-mediated oligomerization in response to light activation. Cluster response is when light and ATP depletion media is added to the environment. Image used in accordance with Creative Commons license CC BY-NC 2.0

LOV domain and Photocaging

Previous research in genetics and biochemical studies in plant and fungus has established a role of LOV domains protein that regulate circadian biology and photochemistry which is used as a base model for the LOV signal transduction. From this established finding comes the concept of photocaging which refers to the use of light to control the activity of a molecule (e.g., a protein or small molecule) by temporarily "caging" it with a photolabile protecting group (Hoffelner et al., 2023). When exposed to light, the cage is removed, restoring the molecule activity. FKF1 (Flavin-binding, Kelch repeat, F-box 1) is a blue light photoreceptor protein in *A. thaliana* which contains a LOV domain. It contains an blue light sensor, a F-box domain and Kelch repeats that mediate protein-protein interactions. Kelch repeats forms a "blade" of the β-propeller fold, consisting of a four-stranded antiparallel β-sheet secondary structure binding with other proteins notably actin filaments of the cell. The LOV domains are photoreceptors that sense environmental light conditions; photoexcitation leads to receptor autophosphorylation and initiation of phototropin signaling (Christie, 2007). These domains, part of the PAS (Per-ARNT-Sim) superfamily, are a group of sensor domains in proteins that help regulate signal transduction, and undergo a conformational change upon absorbing blue light through a flavin mononucleotide (FMN) cofactor enabling them to regulate downstream biological activities (Christie, 2007; Hoffelner et al., 2023). The Per/ARNT/Sim domains (PAS) absorb blue light through the FMN cofactor, which excites the FMN into an active state. This causes the formation of a covalent bond between FMN and a nearby cysteine residue, leading to structural changes in the PAS domain. Over time, the covalent bond breaks, returning the protein to its inactive dark state. This technique allows for the precise manipulation of biological processes by uncaging and activating proteins with light, elucidating cellular events and biochemical pathways (Hoffelner et al., 2023).

CHAPTER 2

Compositional Studies

2.1 *Introduction*

This chapter focuses on further characterizing the composition of OptoProfilin-associated clusters. Given the relationship between focal adhesions and the plasma membrane, and the known role of lipids in compartmentalization and signaling, we first sought to investigate the potential interaction between OptoProfilin focal adhesions and stress-induced condensates and cellular lipid environments using specific fluorescent probes for example LipidSpot 488. We hypothesized that OptoProfilin activation might alter local lipid organization, compared to lipid associations observed in other biomolecular condensates.

We aimed to investigate the associated proteins with OptoProfilin in both non-stressed and stressed states. We focused specifically on key focal adhesions proteins known to reside in distinct layers and that preform different functional roles within the adhesion complex. We examined the localization of paxillin, a core scaffold protein, relative to OptoProfilin structures under both conditions. Subsequently, building on the understanding that focal adhesions have a complex, layered architecture. We extended this compositional analysis to include vinculin and zyxin, proteins involved in linking adhesions to the actin cytoskeleton, mechanotransduction, and stress fiber dynamics.

The central question was whether these focal adhesions proteins remain associated with OptoProfilin upon stress-induced condensate formation, or if there is a differential recruitment or exclusion process, hinting at the potential function of these stress-associated bodies. To address these questions, we employed confocal fluorescence microscopy in HeLa cells expressing

OptoProfilin, utilizing lipophilic dyes, immunostaining, and potentially fluorescent protein fusions to visualize the localization and co-localization of OptoProfilin with lipids and selected focal adhesions proteins under precisely controlled non-stress and osmotic stress conditions combined with blue light activation.

2.2 *Results and Discussion*

Initial investigations into the OptoProfilin system involved assessing the distribution of lipid-specific fluorescent probes in HeLa cells under defined conditions using confocal microscopy **(Figure 2.0)**. This approach aimed to determine if lipids are present in the clusters-induced condensates modulating local lipid environments, potentially by recruiting lipids from their cellular microenvironment, and analogous to lipid interactions observed with endogenous biomolecular condensates such as stress granules, nuclear speckles, and P-bodies. Given that certain mutations in focal adhesion (focal adhesions) proteins, like actin, are known to induce pronounced clustering and alter subcellular distribution, we hypothesized the potential impact of OptoProfilin activation on lipid organization. Surprisingly, fluorescence imaging revealed minimal perturbation in the signal from the lipid-specific dye following blue light-mediated activation of OptoProfilin **(Figure 2.2)**. This observation was unexpected, considering the established, direct involvement of specific lipid compositions and domains (e.g., lipid rafts) in the structural integrity and signaling functions of focal adhesions, which are recognized not merely as adhesive structures but as critical signaling points (Tachibana et al., 2023).

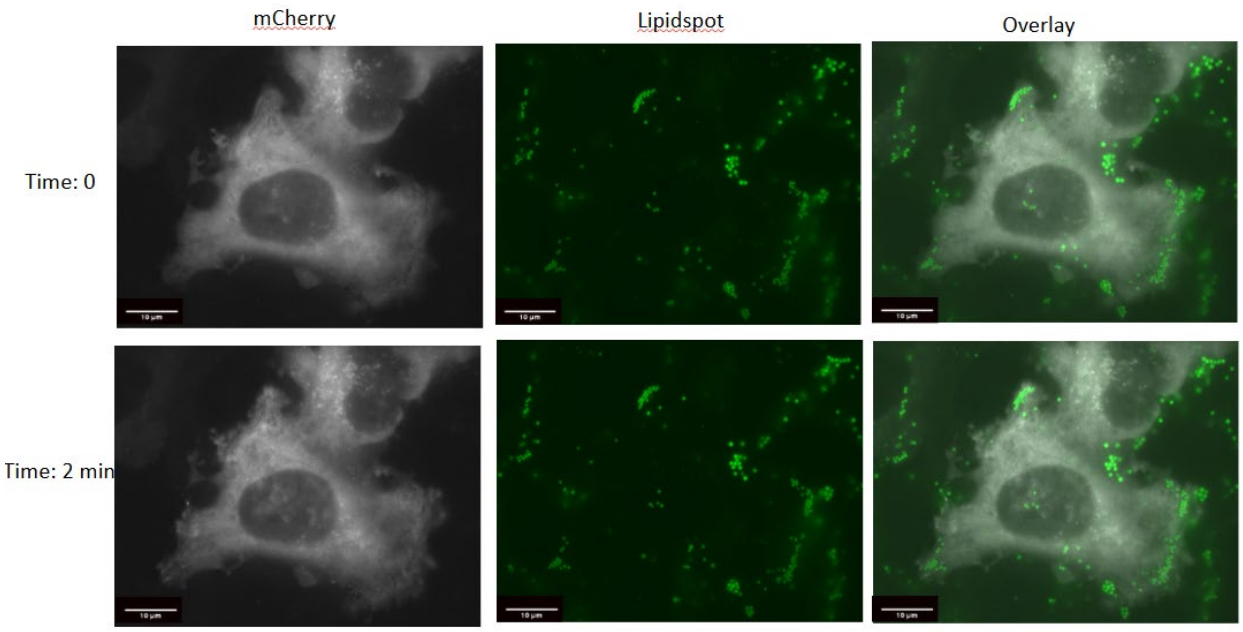

Figure 2.0 OptoProfiln and Lipidspot nonstress condition.
Light activated recruitment of profilin driven by Cry2-mediated oligomerization in response to activation under experimental conditions. HeLa cells were transfected with OptoProfilin constructed using Calfectin and analyzed for light activated localization under non-stress conditions (1X Dulbecco's PBS with Ca and Mg) Lipidspot 488 nm imaged in a separate channel. Imaging sequence: 553 nm (200 ms exposure) and 47 nm (50 nm exposure) pulses applied every 30 s over a 2 min time course.

Subsequently, we investigated the OptoProfilin system's response to stress induced by sorbitol treatment in HeLa cells, aiming to delineate any stimulus-specific localization patterns compared to previously examined conditions. Confocal microscopy revealed that sorbitol treatment consistently elicited a pronounced clustering phenotype of OptoProfilin. When cells were co-incubated with a lipophilic fluorescent dye, OptoProfilin clustering was still observed, yet no discernible co-localization or association between the OptoProfilin clusters and the dye-labeled lipid structures was evident **(Figure 2.1)** and intensity analysis confirmed this finding in **(Figure 2.2)**. It is well-established that cellular lipid homeostasis, encompassing triglycerides

and cholesterol/cholesterol esters is critical. However, the lack of association suggests that the formation of OptoProfilin clusters under osmotic stress does not involve substantial recruitment or sequestration of lipids from the specific compartments highlighted by this dye.

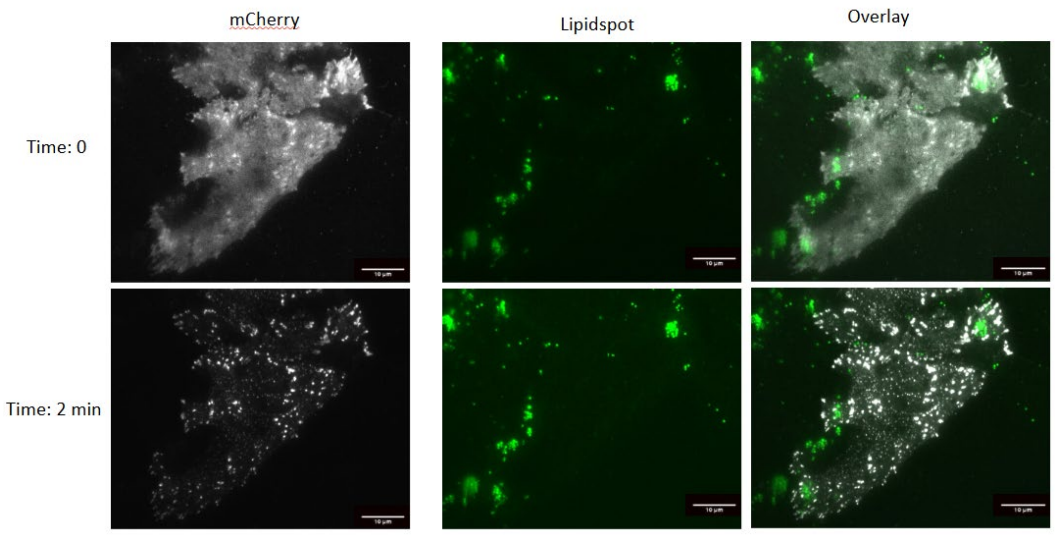

Figure 2.1 OptoProfiln and Lipidspot stress condition.

Light activated recruitment of profilin driven by Cry2-mediated oligomerization in response to activation under experimental conditions. HeLa cells were transfected with OptoProfilin constructed using Calfectin and analyzed for light activated localization under stress conditions Osmotic stress (200 mM Sorbitol, 5 min pre-treatment) Lipidspot 488 nm imaged in a separate channel. Imaging sequence: 553 nm (50 ms exposure) and 47 nm (50 nm exposure) pulses applied every 30 s over a 2 min time course. Scale bar 10 microns.

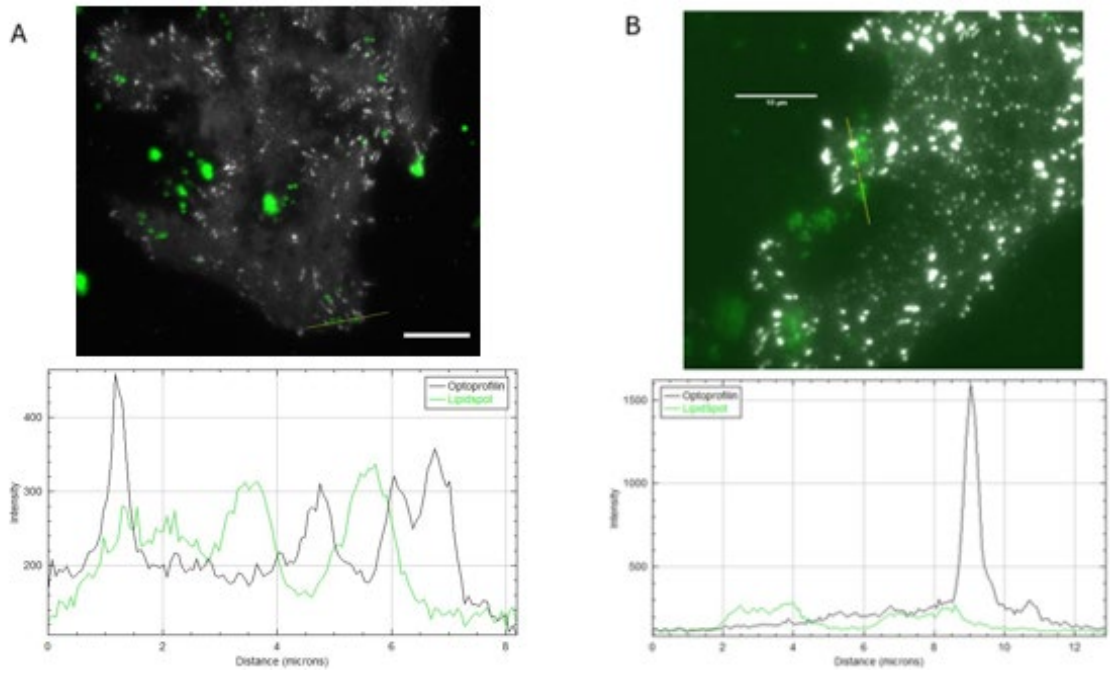

Figure 2.2 Overlay analysis of Optoprofilin and Lipid dye. A. A region of interest (ROI) was selected using a yellow line, as shown in the top panel. Channels were then split to visualize individual signals: the Lipidspot channel (green) and the mCherry-tagged Optoprofilin channel (grayscale). A green line indicates the axis along which fluorescence intensity was measured in the Lipidspot channel, while a black line represents the intensity axis for the Optoprofilin channel. Intensity profiles were generated using the "Plot Profile" function in FIJI by drawing a line across the ROI and extracting pixel intensity values along that line. Prior to colocalization analysis, pixel baseline intensity was adjusted based on background levels in each image. The bottom panel shows the resulting fluorescence intensity profiles over a 2-minute acquisition window. In non-stress conditions, no evidence of lipid internalization was observed upon Optoprofilin activation. **B.** Similar analysis performed under stress-conditioned conditions. The overlay image displays Lipidspot and Optoprofilin signals, and fluorescence intensity plots are shown below. As in panel A, intensity profiles were taken along a ROI. No significant lipid internalization was detected upon Optoprofilin activation under stress. **Scale bar: 10 µm.**

To address the next research question of the composition we wanted to confirm the association of paxillin with focal adhesions and observe it once biomolecular condensate was formed in the presence of stress. Immunostaining for paxillin, a focal adhesion localized protein, was performed using a fixed cell experiment **(Fig. 2.3)**, demonstrating that the co-localization of paxillin with these structures was substantially less prominent and lacked the clear definition observed in the non-stressed focal adhesions context. Qualitative visual assessment of the

resultant morphologies did not, therefore, provide strong evidence for a significant association of paxillin with these stress-induced OptoProfilin condensates. Consequently, to definitively determine the extent of paxillin recruitment to, or exclusion from, these stress-associated structures, further investigation employing rigorous quantitative colocalization analyses is necessary and should be used in further study.

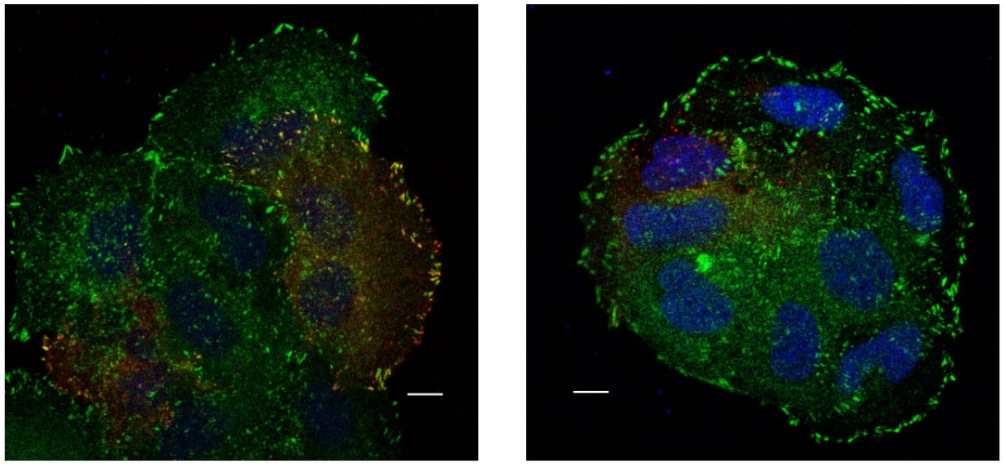

Figure 2.3 OptoProfiln and paxillin nonstress and stress condition in fixed Hela cells. In green is paxillin, red is optoprofilin, and blue is a fluorescent DNA stain DAPI. The left image is a fixed Hela cell that was exposed to PBS conditions. The right image is a fixed Hela cell that was exposed to 2D-G azide solution. Both were stained with anti-paxillin monoclonal antibody. Scale bar 10 micrometers.

Next, vinculin and zyxin GFP fusions were made to study the focal adhesion expression levels within Hela cells **(Figure 2.4)**. The association study was first done so we can view relative expressions within the cell and confirm the construct. Before the transfections took place, we analyzed the transfections for focal adhesion characteristics and abundance of equal DNA transfections using a western blot method and live cell imaging.

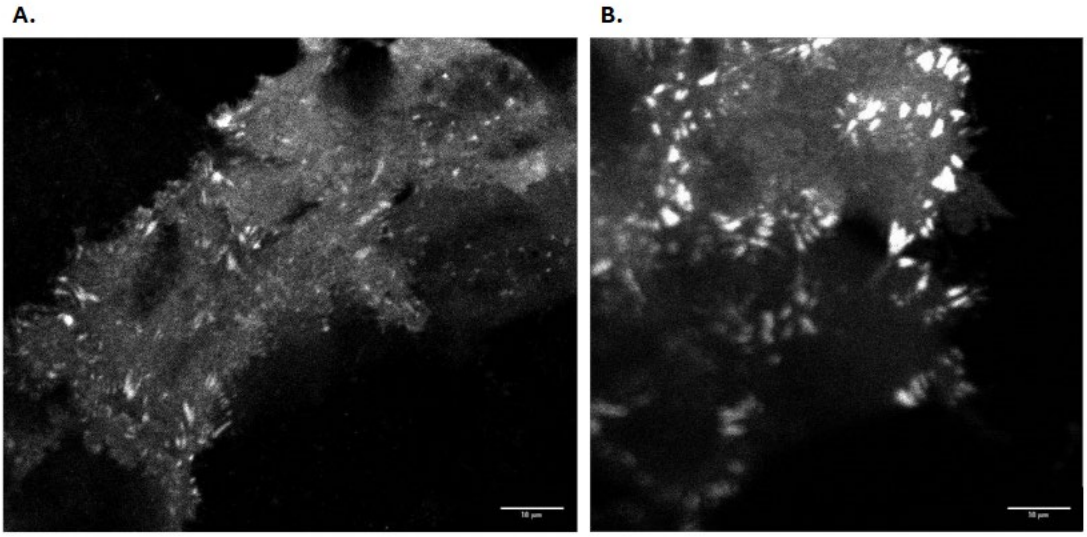

Figure 2.4 Vinculin and Zyxin imaged under GFP channel. A. HeLa cells were transfected with Zyxin-GFP constructed using Calfectin and analyzed for localization. B. HeLa cells were transfected with Vinculin-GFP constructed using Calfectin and analyzed for localization. Scale bar 10 microns

After confirming the focal adhesion phenotype, subsequent experiments investigated the independent effects of stress on Vinculin and Zyxin constructs using the OptoProfilin system under stress. Observation of the mCherry-OptoProfilin channel showed typical recruitment. Examination of the Vinculin GFP channel after 2 minutes of light activation revealed rod-like structures at the focal adhesion sites, coinciding with OptoProfilin recruitment **(Figure 2.5)**. This observation suggests a non-enzymatic function of Vinculin, potentially acting as a signaling factor that recruits other focal adhesion proteins to stabilize force from the extracellular matrix and bind to actin, resulting in the observed rod-like structures.

Under conditions of energetic stress, vinculin displayed trends consistent with those observed under phosphate-buffered saline conditions **(Figure 2.6)**. It is important to note that quantitative analysis was not performed in this study, as the primary objective was to confirm structural alterations and the colocalization of components within stress granule formation. No

colocalization was detected between vinculin and OptoProfilin clusters, suggesting their non-incorporation and involvement in independent stress pathways.

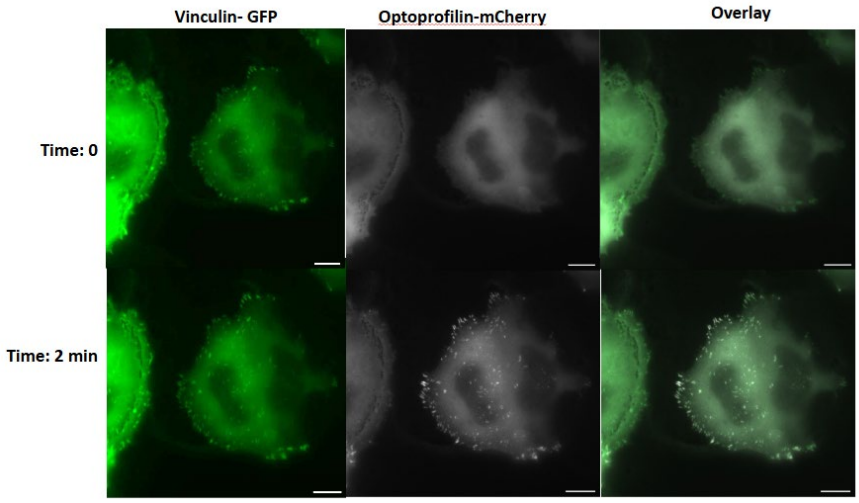

Figure 2.5 Vinculin and OptoProfilin under PBS conditions.
HeLa cells were co-transfected with Vinculin-GFP construct and Cry2-mCherry-OptoProfilin using Calfectin and analyzed for light activated localization under Standard PBS conditions (in 1X Dulbecco's PBS with Ca2+ and Mg2+). Imaging sequence: 553 nm (50 ms exposure) and 470 nm (50 ms exposure) pulses applied every 30 s over a 2 min time course. Scale bars = 10 microns.

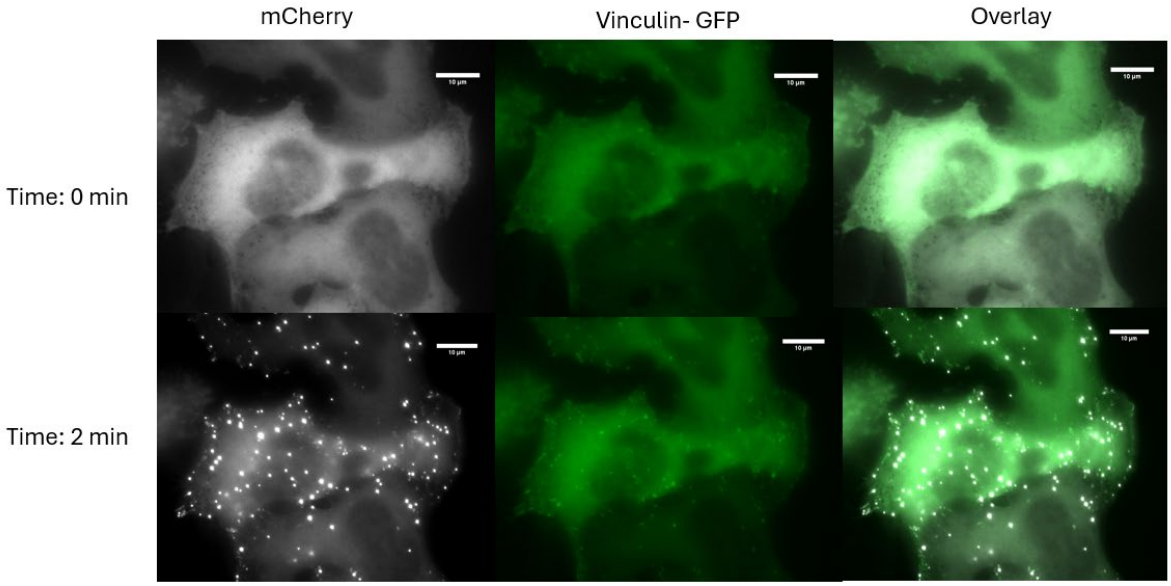

Figure 2.6 Vinculin and OptoProfilin under Stress condition.
HeLa cells were co-transfected with Vinculin-GFP construct and Cry2-mCherry-OptoProfilin using Calfectin and analyzed for light activated localization under Standard stress condition (in ATP-depletion 10 mM NaN3/6 mM 2-DG conditions). Imaging sequence: 553 nm (50 ms exposure) and 470 nm (50 ms exposure) pulses applied every 30 s over a 2 min time course. Scale bars = 10 microns.

Subsequent investigations were conducted on Zyxin, following methodologies analogous to those employed in the vinculin studies. While Vinculin functions as a key structural and mechanical component of focal adhesions, Zyxin possesses a prominent proline-rich domain resembling VASP, which is absent in Vinculin. Consequently, it is hypothesized that the interaction of Zyxin with VASP and the OptoProfilin system will modulate “expected” behavior. As depicted in **(Figure 2.7)**, under non-stress conditions, a consistent pattern emerges wherein the focal adhesion protein VASP and Zyxin is located deeper within the cell, while profilin is situated closer to the cell periphery. Conversely, under stress conditions, an association between the focal adhesion protein and the observed stress granule assembly is evident **(Figure 2.8)**. It

should be noted that not all Zyxin is recruited; however, this observation does not account for the endogenous Zyxin concurrently present within the cell.

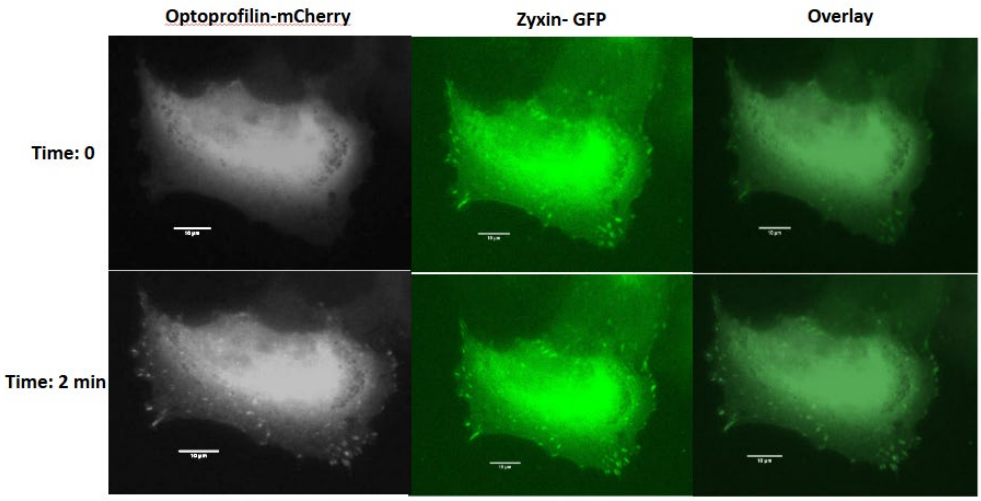

Figure 2.7 Zyxin and OptoProfilin under PBS conditions.
HeLa cells were co-transfected with Zyxin-GFP construct and Cry2-mCherry-OptoProfilin using Calfectin and analyzed for light activated localization under Standard PBS conditions (in 1X Dulbecco's PBS with Ca2+ and Mg2+). Imaging sequence: 553 nm (50 ms exposure) and 470 nm (50 ms exposure) pulses applied every 30 s over a 2 min time course. Scale bars = 10 microns.

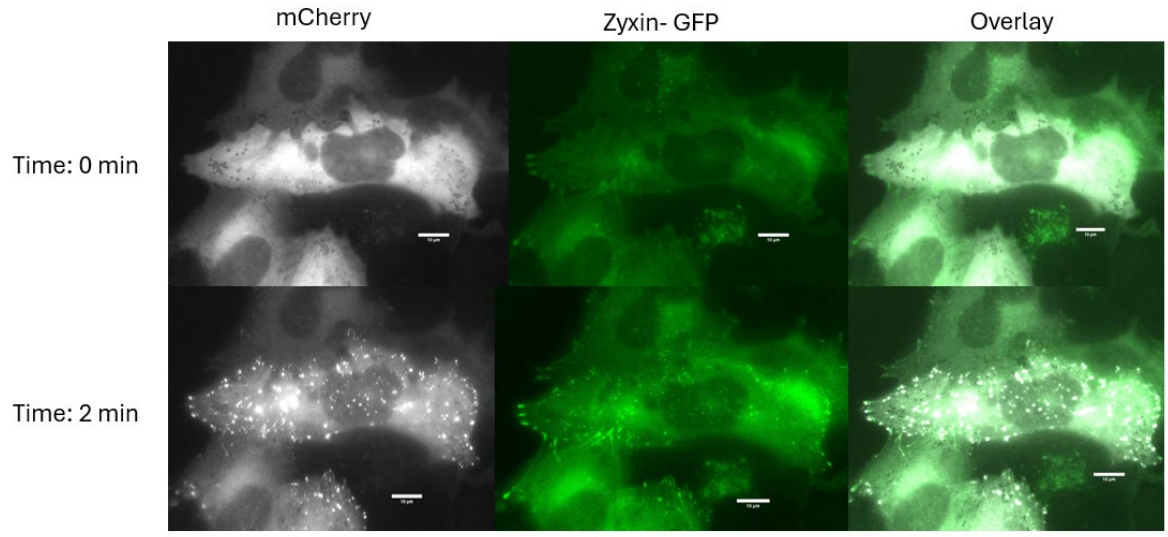

Figure 2.8 Zyxin and OptoProfilin under stress conditions.
HeLa cells were co-transfected with Zyxin-GFP construct and Cry2-mCherry-OptoProfilin using Calfectin and analyzed for light activated localization under Standard stress conditions (in ATP-depletion 10 mM NaN3/6 mM 2-DG conditions). Imaging sequence: 553 nm (50 ms exposure) and 470 nm (50 ms exposure) pulses applied every 30 s over a 2 min time course. Scale bars = 10 microns.

The differential sorting of Vinculin excluded and Zyxin included into the stress-induced condensates suggests these are not simply non-specific aggregates but rather possess a degree of compositional specificity dictated by the cellular state and protein-protein interactions modulated by stress. Vinculin's role in linking integrins to the actin cytoskeleton and mechanotransduction might be less central to the function of these specific stress condensates, or perhaps its association with focal adhesions is stabilized differently, preventing incorporation.

Zyxin, known for its role in actin filament organization, mechanosensing, and stress fiber repair, particularly its LIM domain-mediated interactions, appear to be actively recruited or preferentially partitioned into these OptoProfilin structures under stress. This suggests the OptoProfilin condensates might function as hubs for stress-related cytoskeletal reorganization,

potentially involving Zyxin-mediated pathways. The distinct behavior of Vinculin and Zyxin underscores the complexity of focal adhesions protein dynamics during the cellular stress response and warrants further investigation into the specific interaction mechanisms.

Table 2.2: Table of results from Chapter 2

Name	Condition	Incorporated into Condensates under stress, focal adhesions in PBS
Zyxin/ Optoprofilin	Stress	Yes
	PBS	Yes
Vinculin/ Optoprofilin	Stress	Yes
	PBS	Yes
Lipidspot / Optoprofilin	Stress	No
	PBS	No
Paxillin/ Optoprofilin	Stress	No
	PBS	Yes

2.3 Methods and Materials

Cell lines and Transfection

Cell lines and transfection Miniprep quantities of DNA of each construct were created from E. coli and collected for cell transfection. Transfection of HeLa cells was then performed with Calfectin reagent (SignaGen) following manufacturer's suggested protocols. Briefly, for dual transfections in 35 mm glass bottom dishes, plasmid DNA was combined in a 1:1 ratio (1,250 ng per plasmid for dual transfections) in 100 µl of DMEM, followed by the addition of 3

µl of Calfectin reagent. The solution was allowed to incubate at room temperature for 10 min, followed by dropwise addition to cell culture. Transfection solutions were allowed to remain on cells overnight. Cells were maintained at 37°C and 5% CO2 in a humidified tissue culture incubator, in culture medium consisting of DMEM supplemented with 10% FBS and 1% Penicillin-Streptomycin

Lipid Spot Protocol

HeLa cells were cultured in Eagle DMEM until they reached 70-80% confluency. Cells were transfected with OptoProfilin construct using a suitable transfection method mentioned above (e.g. Lipofectamine). After transfection, the cells will be incubated with Lipid Spot Dye (Biotium) following the manufacturer's instructions to stain lipid domains. OptoProfilin was activated in the transfected cells by light illumination. Exposure times were set at 150 ms (GFP, 470 42 nm) and 300 ms (mCherry, 550 nm), with LED light sources at 50% power, and images acquired every 30 seconds over a 10 min time course.

Imaging

Confocal Microscopy: Confocal images of fixed cells were obtained with Olympus IX2-DSU tandem spinning disk confocal laser scanning microscope or with a Zeiss LSM 880 microscope with Airyscan technology. Fluorescence images were colorized and overlaid using FIJI software.

Widefield Microscopy: A Leica DMi8 Live Cell Imaging System, equipped with an OKOLab stage-top live cell incubation system, LASX software, Leica HCX PL APO 63x/1.40-0.60na oil objective, Lumencor LED light engine, CTR advanced+ power supply, and a Leica

DFC900 GT camera, was used to acquire images. Exposure times were set at 150 ms (GFP, 470 42 nm) and 300 ms (mCherry, 550 nm), with LED light sources at 50% power, and images acquired every 30 seconds over a 10 min time course.

Fixed cell experiments

Transfected HeLa cells were washed with Dulbecco's PBS (with calcium and magnesium; 3 x 1 mL), prior to treatment with ATP depletion medium (6 mM D-Deoxyglucose and 10 mM Sodium Azide in Dulbecco's PBS) for the indicated time intervals. ATP depletion medium was removed by aspiration, cells washed gently (1X with 1 mL Dulbecco's PBS), then. fixed for 45 min with pre-warmed 4% paraformaldehyde solution (37oC; prepared from 16% PFA (Electron Microscopy Sciences and DPBS) at room temperature for 45 min. Following fixation, cells were washed with PBS, then permeabilized for 3 min using pre-chilled methanol (-20oC). Methanol was removed by aspiration, then cells were blocked for 30 min with antibody. dilution buffer (30 µl Triton X-100, 0.1 g of BSA, 10 mL of Dulbecco's PBS). Cells then were. incubated overnight at 4 ºC with primary antibody (anti-Actin (Santa Cruz); 1:500 in antibody. dilution buffer). The following day, the primary antibody solution was removed by pipette, and cells were washed three times with Dulbecco's PBS. Cells were incubated with Alexa 488 conjugated goat anti-mouse secondary (Invitrogen; 1:200 in antibody dilution buffer) for 1 hour at room temperature, followed by a Dulbecco's PBS wash (1 mL; 3 x 5 min). Cells were stored in Dulbecco's PBS prior to imaging.

CHAPTER 3

VASP AND OPTOPROFILIN MUTAGENISIS STUDIES

3.1 Introduction

The study of protein complexes and biomolecular condensates has gained significant traction in recent years due to their implications in various physiological and pathological states. Aberrant phase transitions and condensate dysregulation have been linked to numerous diseases, including cancer and neurodegenerative disorders. Understanding the mechanisms governing condensate formation, dynamics, and function is therefore crucial for elucidating disease pathogenesis and developing potential therapeutic strategies. To explore how different ligand parameters such as affinity, valency, amino acid composition, and charge can tune condensate dynamics, mutagenesis has been used to employ a research catalog of peptide characterization studies from different aberrant proteins discovered.

Traditional methods for studying condensates, such as using 1,6-hexanediol, often lack specificity and has limitations (Brumbaugh-Reed, 2024). 1,6-hexanediol is an aliphatic alcohol. It has both hydroxyl groups and an aliphatic chain, allowing it to interact with both polar and hydrophobic residues within proteins and nucleic acids. By doing so, it weakens the non-covalent, weak hydrophobic interactions such as π-π stacking and hydrophobic contacts that mediate the assembly of many condensates. While recent approaches, like the DISCO system which relies on the use of chemical dimerizers to inducibly recruit a ligand to the condensate-forming protein, triggering condensate dissociation (Hernandez-Candia et al., 2021). This offers a more targeted dissolution but still face limitations in terms of speed and spatial control. Optogenetic tools, however, provide a promising avenue for manipulating condensates with high precision. By leveraging light-sensitive proteins, we can induce or disrupt condensate formation

in a controlled manner, allowing for detailed investigation of their roles in cellular function to explore how different ligand parameters can tune condensate dynamics (Zhu J,2021).

This chapter will focus on mutating certain residues to explore their roles in condensate formation. In the first region of VASP is the EVH1 domain responsible for the abl tyrosine kinase, a non-receptor tyrosine kinase, also known as ABL1. These domains function by helping cells maintain their shape and move, aiding in the uptake of molecules, participating in cellular recycling (autophagy), responding to DNA damage, and even influencing programmed cell death. It achieves this by adding phosphate groups to various proteins, thereby controlling their activity.

The first mutation is L1234 in profilin; which is to be positioned in a hydrophobic residue pocket that is surrounded by rich hydrogen bonding leucine provides a smaller less reactive side chain that can disrupt those stability interactions and can allow the alpha helix to move more freely in the matrix. Live cell imaging can potentially allow the observation of disruption of the secondary structure well enough to cause phenotype induced cell responses that carry weight on the outcome of formation of condensates. Application of site directed mutagenesis can show a need for the study of residue specific mutations on the significance in cellular biology and chemical environment in disease. The second profilin mutation is H134; it is located in an exposed position outside the alpha helix that interacts with an alpha helix proline on the VASP domain. This mutant causes inter- and intra-structural stability to a tyrosine in addition to the surrounding solvent stability. Being a positively charged amino acid, its highly positively charged hydrophilic mutation to alanine can be used to induce change in folding and stability.

Table 3.1 VASP and Profilin Residues Chosen for This Study.

Mutation Name	Proposed Impact
VASP-Y39A	Abl Tyrosine Kinase Inhibition
VASP-P120E	VASP PPR region
VASP-L209E	VASP Binding to Profilin Site
Profilin_L123A	C-Terminus Alpha Helix affinity to PPR
Profilin_H134A	C-Terminus Alpha Helix affinity to PPR

3.2 Results and Discussion

For our control studies of the profilin; mutant S138E confirms the importance of this mutation on the effects inhibitor of VASP-profilin binding. This identified a phosphorylation site that proved the reported results that the construct that we created Cry2.Pro.S138E did not recruit to focal adhesions while the Cry2.Pro.S138A did. To take a step further we looked at mutations on VASP starting with previous literature precedent on "key" sites that are required for protein activation and localization. Y39A was the first mutation of interest located as previously mentioned on the EVH1 domain, being a non-receptor tyrosine kinase regulated by post-translational modification and binding partners leading to a cascade.

Initial imaging of the Y39A in Hela cells shows a non-localization pattern which is expected to be seen as previous literature suggests (Döppler H, 2013). Which is shown in **(Figure 3.1)** Adding the optogenetic system in the presence of light activation, we see minimal change. This result suggests that the Y39A mutation is sufficient to prevent VASP localization, even when subjected to light-induced recruitment by the optogenetic system, highlighting the critical nature of this residue for EVH1 domain function.

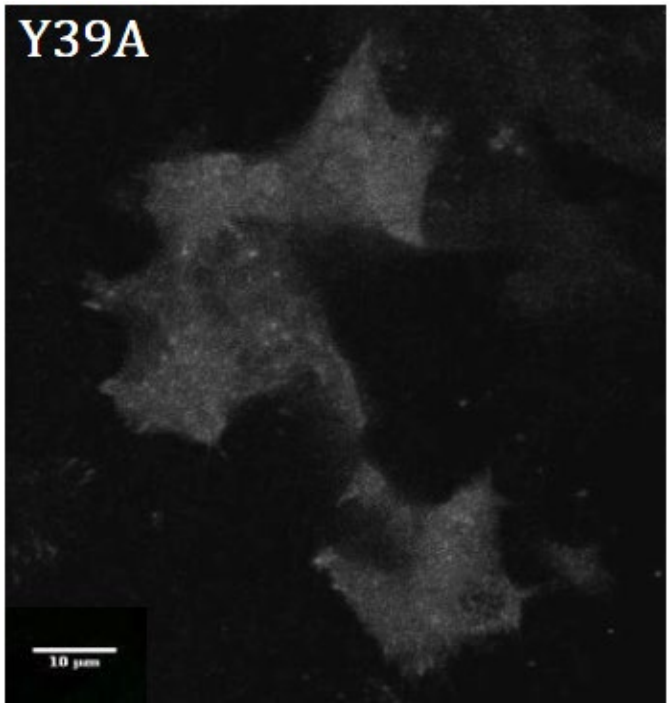

Figure 3.1: Fluorescence imaging of mutant Y-39 in HeLa cell. Greyscale micrograph of a HeLa cell expressing the Y39A mutant protein. The image is a cropped region selected to show representative localization.

Based on initial investigations demonstrating a non-localization pattern of OptoProfilin, it can be definitively concluded that the abl domain on VASP significantly influences the intracellular localization of VASP. In furtherance of the investigation, it was decided to examine how activation of the optogenetic switch and/or stress affects this mutation and whether a recovery or a complete loss of function could be observed in this mutation **(Figure 3.1)**.

In phosphate-buffered saline (PBS) after two minutes of light activation and subsequent imaging, a loss of OptoProfilin function and VASP was observed **(Figure 3.2)**. When a co-localization assay was performed, the regions of OptoProfilin and VASP that appeared to overlap were suspected to be due to background intensity of the OptoProfilin and VASP in the imaged

cell **(Figure 3.3).** The majority of cells did not exhibit an association. Conversely, the expression under stress conditions showed a gain of focal adhesions after two minutes of blue light activation with low OptoProfilin expression. However, when observing the lamellipodia using the co-localization tool in a well co-transfected cell, it was observed that there was no association of the mutant with the OptoProfilin system. The response was not as robust as compared to the wild-type (WT) and suggests that the stress response may be a multi-level factor that can be altered due to potential stress by the environment and the protein folding during cell development progression **(Figure 3.4).** Notably, focal adhesions located closer to the nucleus had a more prominent effect on the location and were observed to function in some cells where OptoProfilin was present. Colocalization test was performed on the stress cells and Optoproflin intensity was higher than GFP when looking at the cell edge and a cluster of focal adhesions **(Figure 3.5).** This Indicates that stress had an opposite reaction when looking at a typical response of this optogenetic system. These results indicate a complex interplay between the Y39A mutation, light activation, and stress conditions in regulating VASP and OptoProfilin localization and function. It was also found that the correlation between the two was 0.25 +/- 0.1 indicating a weak correlation between the two proteins.

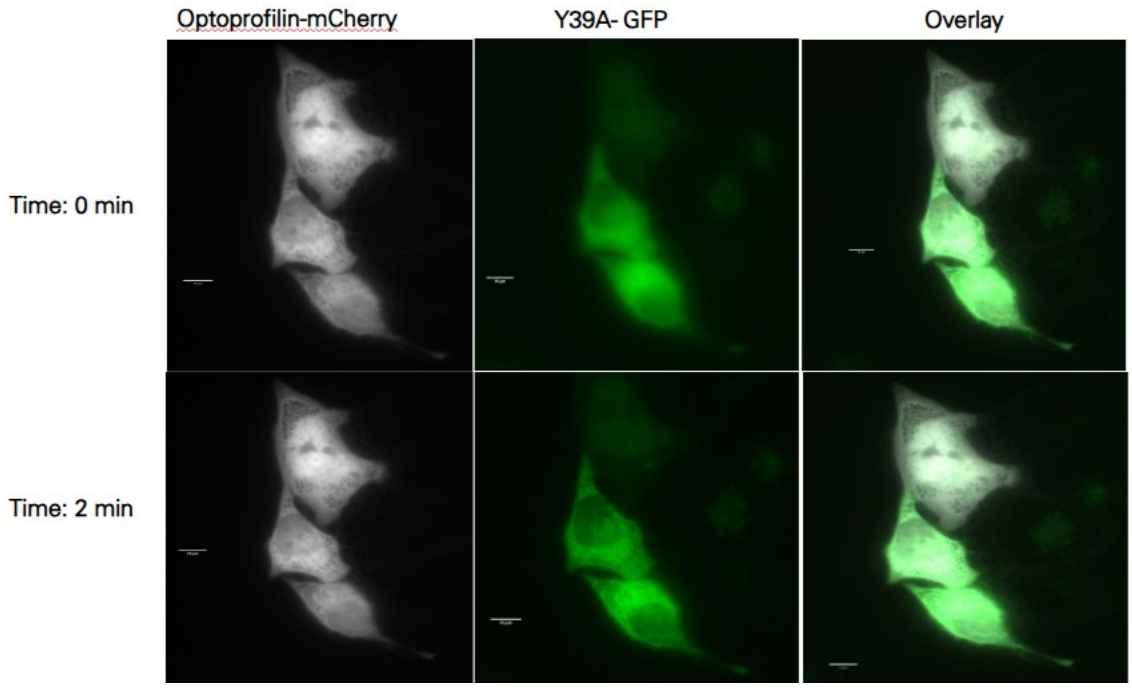

Figure 3.2: **Recruitment profile of VASP Y-39 mutant to focal adhesions in HeLa cell under non-stress conditions.** Absence of recruitment of OptoProfilin to focal adhesions in HeLa cells under non-stress conditions. HeLa cells were co-transfected with Y39A constructs and Cry2-mCherry-profilin using Calfectin 31 and subjected to light-activated localization analysis in 1X Dulbecco's PBS supplemented with Ca2+ and Mg2+. Imaging protocol: 553 nm (50 ms exposure) and 470 nm (50 ms exposure) pulsed illumination every 30 seconds over a 2-minute duration. Scale bars represent 10 microns.

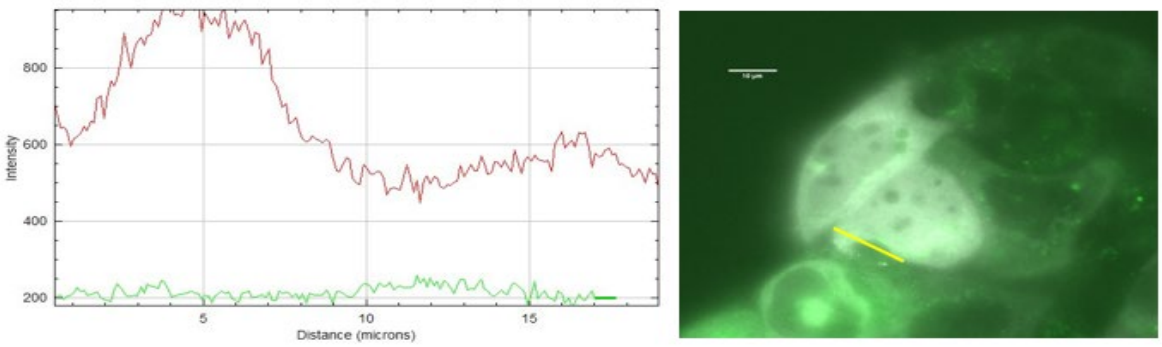

Figure 3.3 Image analysis of VASP Y-39 fluorescence intensity colocalization with overlay PBS condition. This analysis was performed on a selected region of Y39. The image is presented in the overlay with the ROI selected, it represents a composite of multiple channels. The left image demonstrates the overlapping fluorescence intensity of GFP and mCherry graph, yielding a Pearson's correlation coefficient of 0.15. Right Image shows the portion selected for the test outlined.

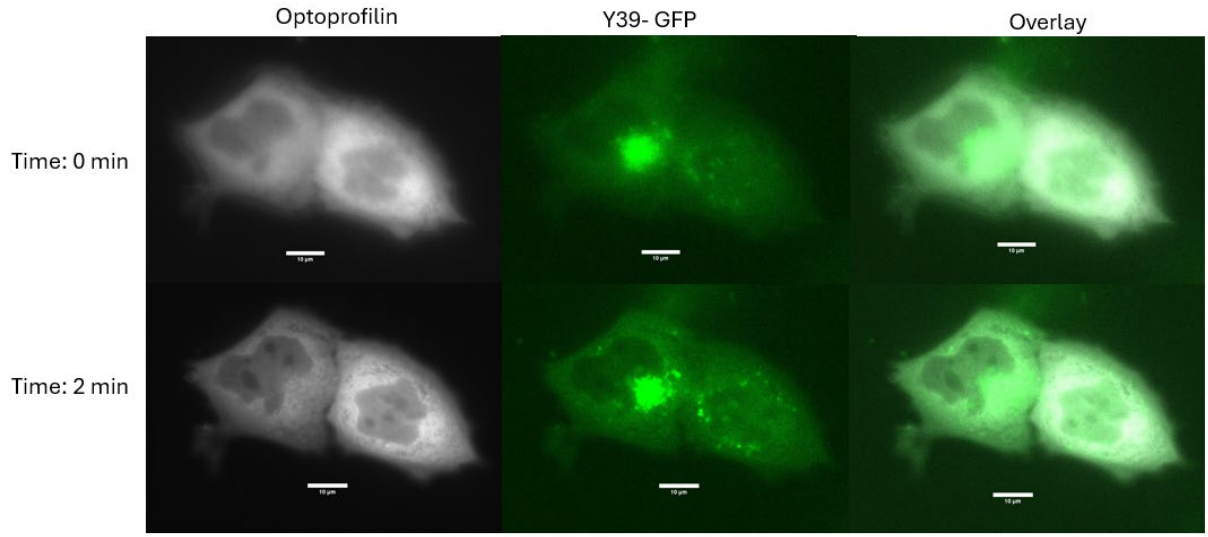

Figure 3.4: **Recruitment of VASP Y-39 mutant to biomolecular condensates in HeLa cells under stress conditions.** HeLa cells were co-transfected with Y39A construct and Cry2-mCherry-profilin using Calfectin 31 and subjected to light-activated localization analysis under energetic stress conditions (6 mM 2-DG and 10 mM NaN3 in 1X Dulbecco's PBS with Ca2+ and Mg2+). Imaging protocol: 553 nm (50 ms exposure) and 470 nm (50 ms exposure) pulsed illumination every 30 seconds over a 2-minute duration. Scale bars represent 10 microns.

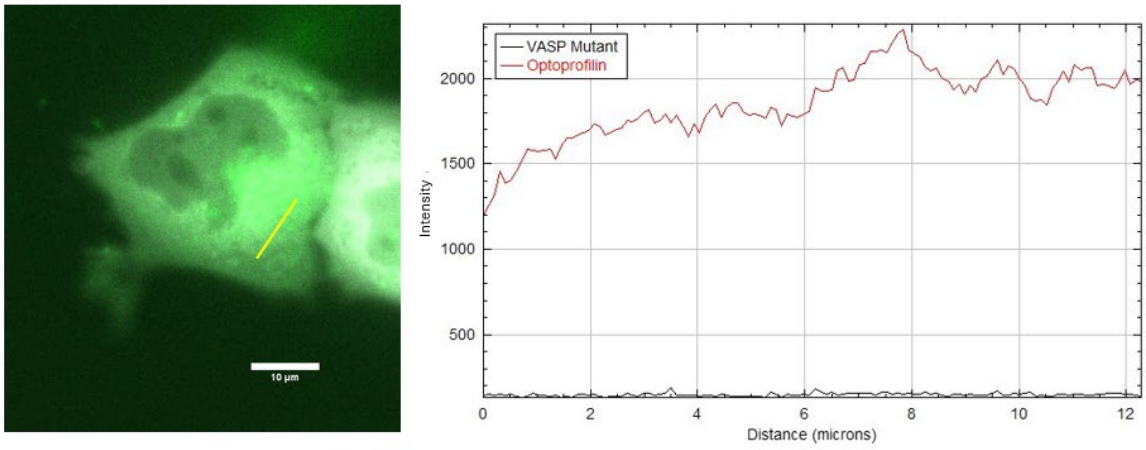

Figure 3.5 Image analysis of VASP Y-39 fluorescence intensity colocalization with overlay stress condition. This analysis was performed on a selected region containing a group of Y39A condensates. While the image is depicted in overlay for visual clarity, it represents a composite of multiple channels. The left image demonstrates the overlapping fluorescence intensity of GFP and mCherry channels, yielding Pearson's correlation coefficient of 0.25. Right Image shows the portion selected for the test outlined in a box.

The single amino acid substitution of proline to glutamic acid at position 120 (P120E) within the VASP protein was previously examined. This specific mutation resides within the polyproline-rich domain of VASP, a region known to be crucial for mediating interactions with other cellular proteins, particularly those involved in cytoskeletal regulation and cell adhesion. Expression studies were conducted using HeLa cells as a model system previously like the Y39A point mutation. The results of these expression analyses demonstrated that the P120E variant of VASP was indeed capable of being recruited to focal adhesions within HeLa cells **(Figure 3.6)**. Furthermore, this localization pattern was observed to be qualitatively like that of the wild-type VASP protein, suggesting that despite the amino acid change in the polyproline region, the P120E mutant retained the ability to target these crucial cellular structures. This finding implies that the P120E mutation, at least in the context of focal adhesion recruitment in HeLa cells, does not abolish a primary targeting signal or severely disrupt the overall protein conformation required for this localization **(Figure 3.7)**. Compared with the addition of the optogenetic switch which showed comparable results in a 0.85 Pearson's correlation from the fluorescence intensity overlay on an in-line test. A finding which shows a strong association that this point mutation under normal conditions performs as expected **(Figure 3.8)**.

Cells expressing both endogenous VASP and the P120E mutation, when subjected to stress and light activation, demonstrated a clustering response analogous to that observed in wild-type VASP and Optoproflin co-transfection **(Figure 3.9)**. The absence of substantial alteration compared to the Y39A with this proline mutation may be attributed to the alpha helix maintaining adequate solvent stability, thereby enabling protein translocation to the target upon binding. Upon doing a colocalization test on the overlay it shows that the fluorescence intensity of the optogenetic system outpowers the binding of VASP to and conveys a low intensity of

incorporation of the clusters potentially signaling that this mutation has some effect on the affinity to stay at focal adhesions rather than to disassociate into the biomolecular condensates altering the microenvironment of this protein side chain **(Figure 3.10)**. Co-localization testing under stress showed that although there was an increase in the amount of VASP at sites of biomolecular condensates, they were colocalized well by the indication of a yellow glow from the site after 2 minutes.

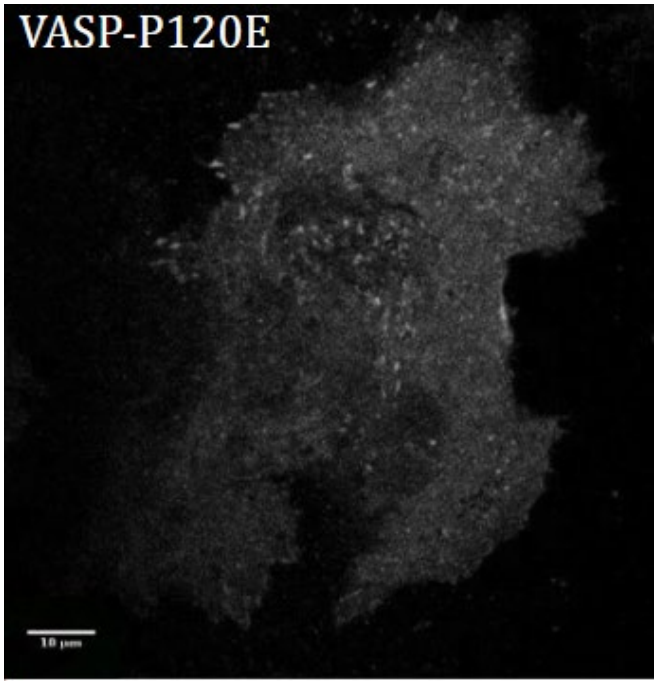

Figure 3.6: **Fluorescence imaging of mutant P-120 in HeLa cell.** Greyscale micrograph of a HeLa cell expressing the P120E mutant protein. The image is a cropped region selected to show representative localization. Scale bar 10 microns.

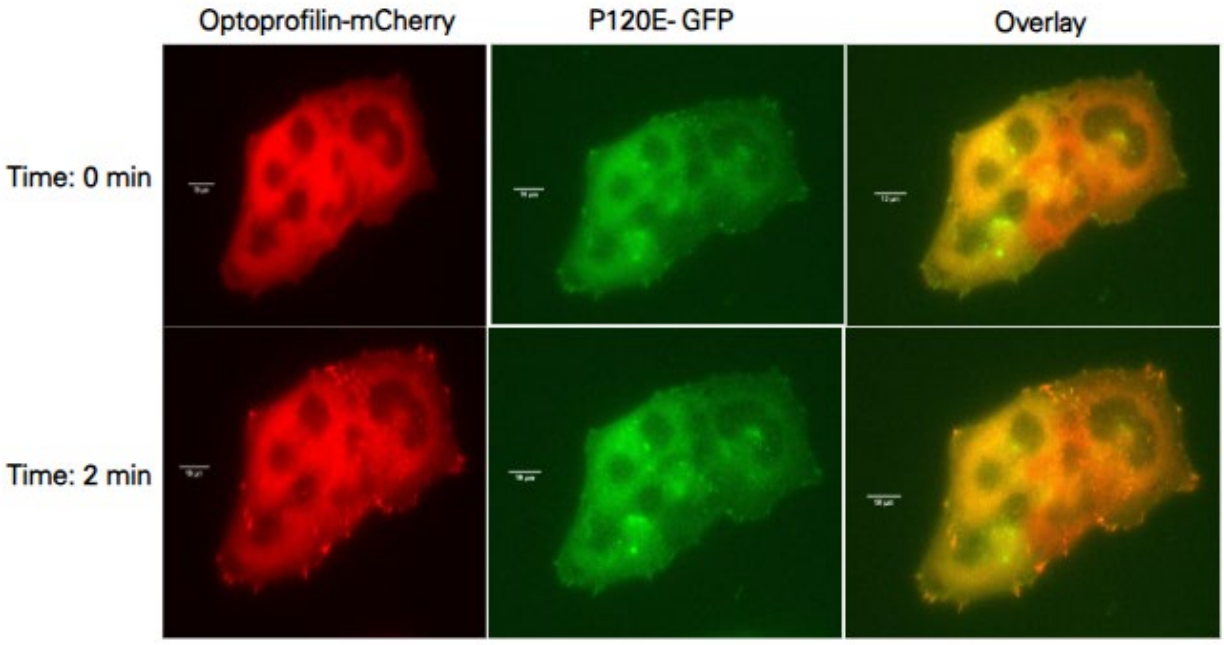

Figure 3.7: **Recruitment profile of VASP P-120 mutant to focal adhesions in HeLa cell under non-stress conditions.** HeLa cells were co-transfected with VASP-P120E construct and Cry2-mCherry-profilin using Calfectin 31 and subjected to light-activated localization analysis in 1X Dulbecco's PBS supplemented with Ca2+ and Mg2+. Imaging protocol: 553 nm (50 ms exposure) and 470 nm (50 ms exposure) pulsed illumination every 30 seconds over a 2-minute duration. Scale bars represent 10 microns.

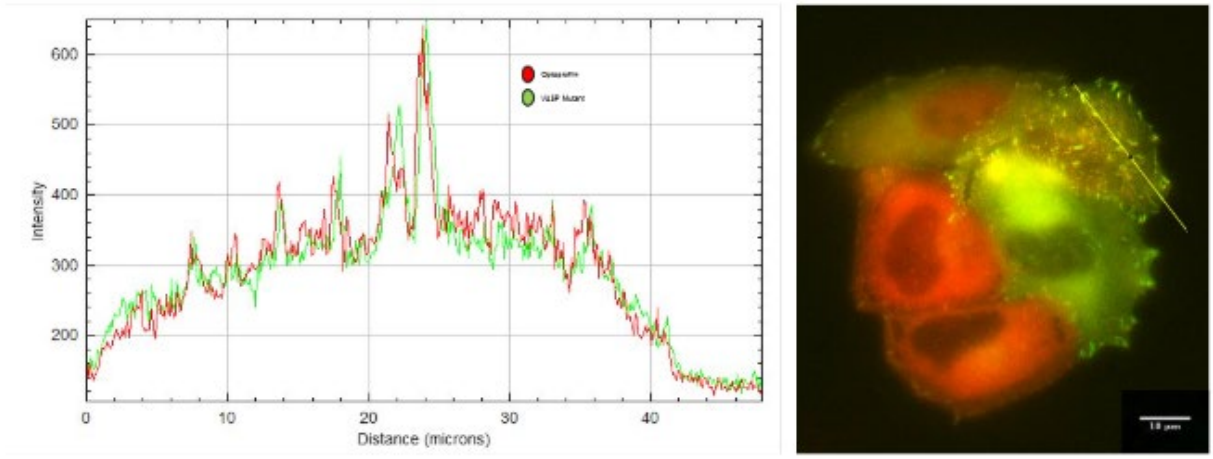

Figure 3.8: Image analysis of VASP P-120 fluorescence intensity colocalization with overlay PBS condition. Colocalization graph of the P120 mutant and OptoProfilin on the left. Overlay of the focal adhesion area selected on the right. This analysis was performed on a selected region containing a group of P120E focal adhesions. While the image is depicted in the overlay channel for visual clarity, it represents a composite of multiple channels. The left image demonstrates the overlapping fluorescence intensity of GFP and mCherry, yielding a Pearson's correlation coefficient of 0.85. Right Image shows the portion selected for the test outlined in a line.

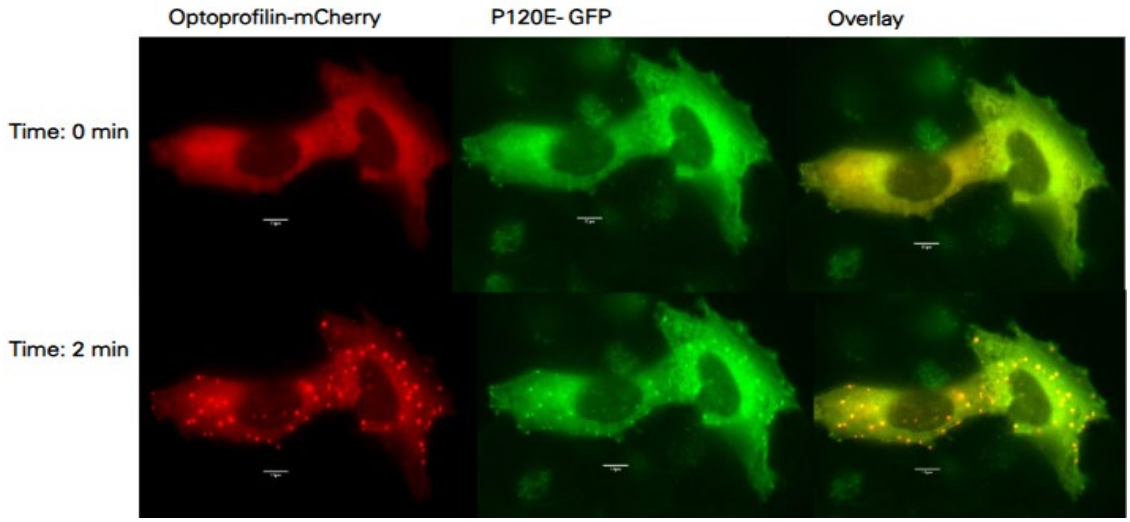

Figure 3.9: **Recruitment of VASP P-120 mutant to biomolecular condensates in HeLa cells under stress conditions**. HeLa cells were co-transfected with VASP-P120E construct and Cry2-mCherry-profilin using Calfectin 31 and subjected to light-activated localization analysis under energetic stress conditions (6 mM 2-DG and 10 mM NaN3 in 1X Dulbecco's PBS with Ca2+ and Mg2+). Imaging protocol: 553 nm (50 ms exposure) and 470 nm (50 ms exposure) pulsed illumination every 30 seconds over a 2-minute duration. Scale bars represent 5 microns.

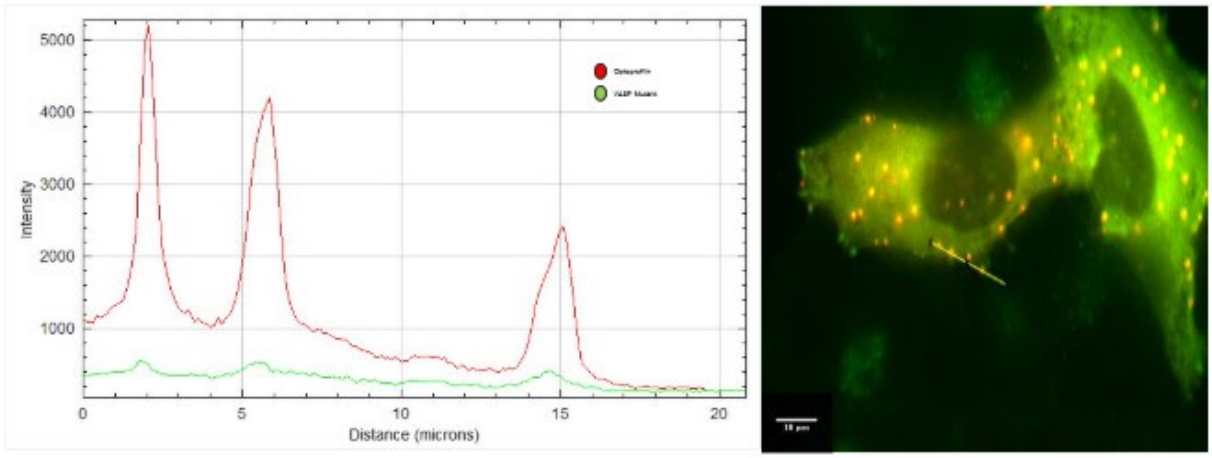

Figure 3.10: **Image analysis of VASP P-120 fluorescence intensity colocalization with overlay stress condition.** This analysis was performed on a selected region containing a group of P120E condensates. While the image is depicted in the Overlay channel for visual clarity, it represents a composite of multiple channels. The left image demonstrates the overlapping fluorescence intensity of GFP and mCherry, yielding a Pearson's correlation coefficient of 0.85. Right Image shows the portion selected for the test outlined in a box. Scale bar = 10 microns

The L209E mutation, positioned at a site potentially interacting with the first tyrosine residue of profilin and thus affecting alpha helix stability, was introduced. Initial expression studies in HeLa cells revealed localization at focal adhesions, suggesting a non-disruptive phenotype for this mutation **(Figure 3.11)**. Analysis of the L209E PBS mutation following OptoProfilin system activation demonstrates profilin localization to the cell membrane and focal adhesions after 2 minutes **(Figure 3.12)**. Notably, on first glance this mutation appears to enhance OptoProfilin localization upon activation forming sharper focal adhesions. It is hypothesized that the glutamic acid mutation induces a conformational change in the alpha helical structure, potentially facilitating tighter profilin binding due to altered oligomerization.

In the absence of stress and under blue light activation alone, the mutation facilitated the recruitment of OptoProfilin to focal adhesions, where it exhibited colocalization. Graphical

analysis **(Figure 3.13)** revealed that VASP intensity was approximately twice that of OptoProfilin. Comparative analysis with the wild type demonstrated a similar phenotypic response. Observation of VASP behavior suggests its localization atop profilin, potentially indicating a closer proximity of VASP to the outer cell wall **(Figure 3.12)**.

L209E in the presence of stress did show a moderate correlation to the clustering phenotype and when analyzed using the colocalization test after two minutes in **(Figure 3.14)** and **(Figure 3.15)**. When we looked at the correlation it was minimal to none. When analyzing a group of cells all cells had a clustering phenotype, both VASP and Optoprofilin were present.

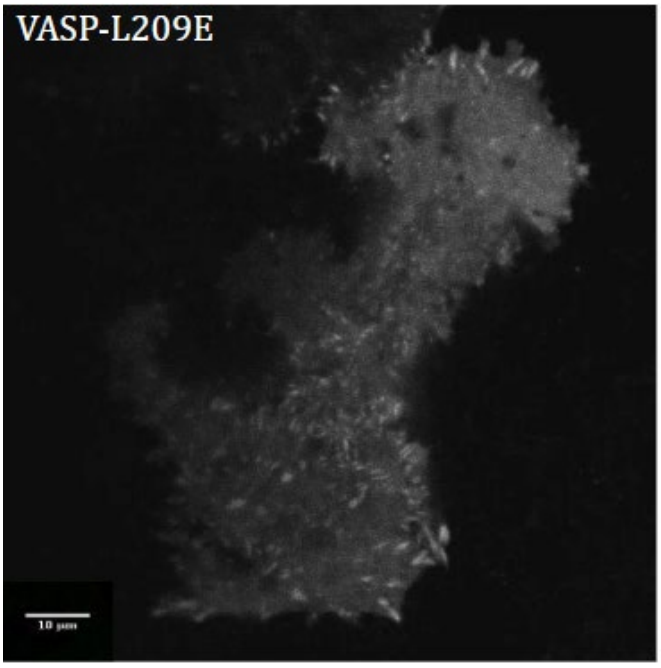

Figure 3.11: **Fluorescence imaging of mutant L-209 in HeLa cell.** Greyscale micrograph of a HeLa cell expressing the L209E mutant protein. The image is a cropped region selected to show representative localization.

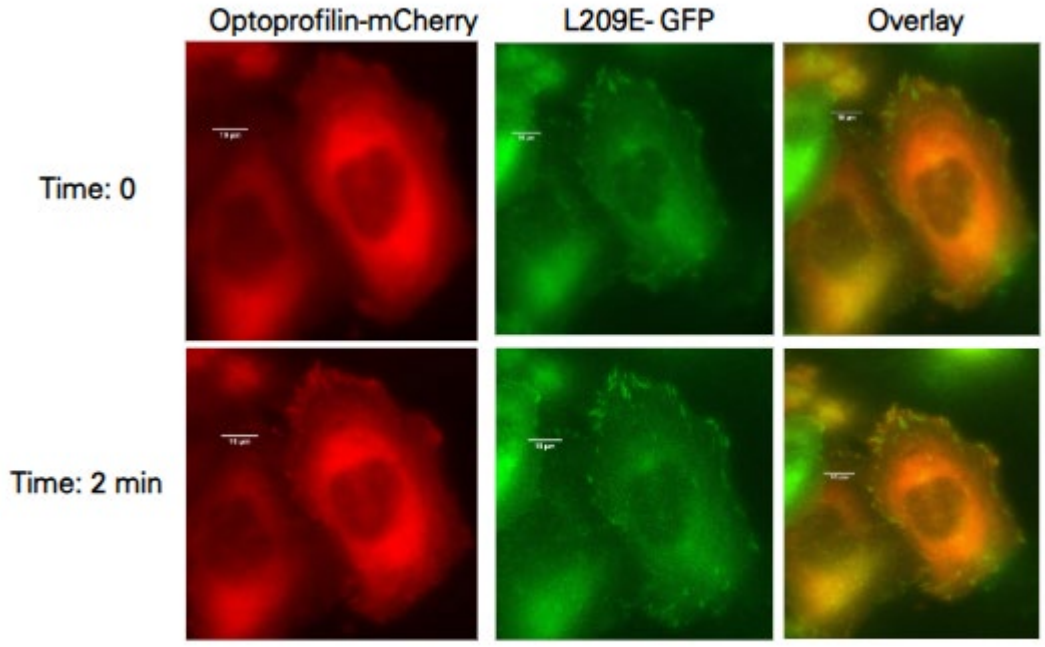

Figure 3.12: **Recruitment profile of VASP L-209 mutant to focal adhesions in HeLa cell under non-stress conditions.** HeLa cells were co-transfected with VASP-L209E construct and Cry2-mCherry-profilin using Calfectin 31 and subjected to light-activated localization analysis in 1X Dulbecco's PBS supplemented with Ca2+ and Mg2+. Imaging protocol: 553 nm (50 ms exposure) and 470 nm (50 ms exposure) pulsed illumination every 30 seconds over a 2-minute duration. Scale bars represent 10 microns.

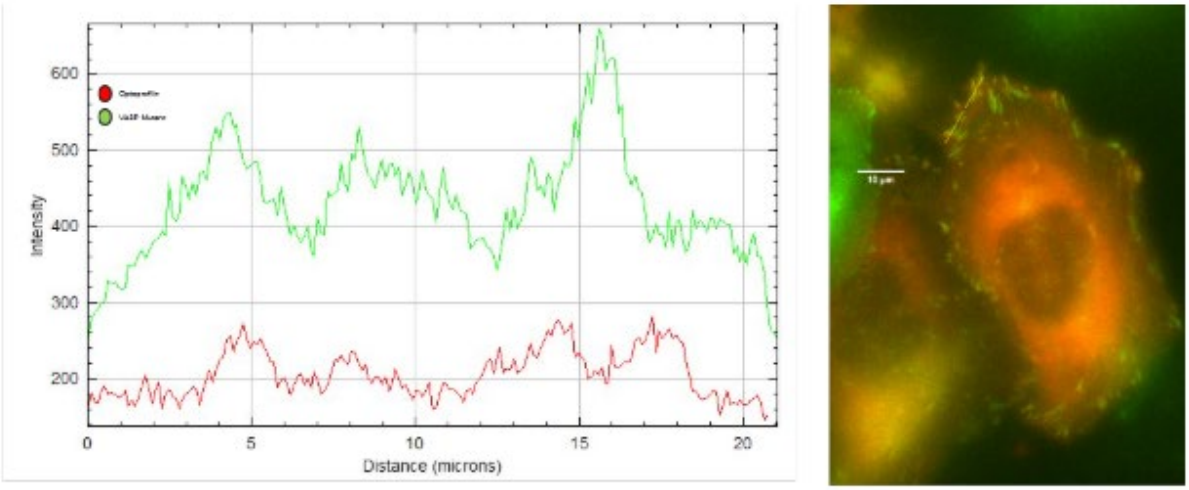

Figure 3.13: Image analysis of L-209 fluorescence intensity colocalization with overlay PBS condition This analysis was performed on a selected region containing a group of L209E focal adhesions. While the image is depicted in the overlay channel for visual clarity, it represents a composite of multiple channels. The left image demonstrates the overlapping fluorescence intensity of GFP and mCherry, yielding Pearson's correlation coefficient of 0.82. Right Image shows the portion selected for the test outlined in a box. Scale bar 10 microns

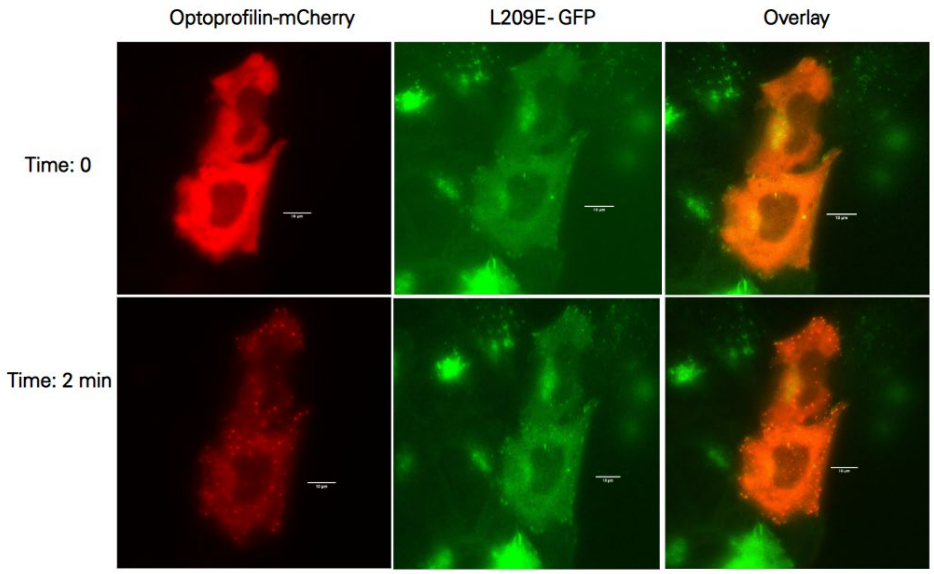

Figure 3.14 Recruitment of VASP L-209 mutant to biomolecular condensates in HeLa cells under stress conditions. HeLa cells were co-transfected with VASP-L209E construct and Cry2-mCherry-profilin using Calfectin 31 and subjected to light-activated localization analysis under energetic stress conditions (6 mM 2-DG and 10 mM NaN3 in 1X Dulbecco's PBS with Ca2+ and Mg2+). Imaging protocol: 553 nm (50 ms exposure) and 470 nm (50 ms exposure) pulsed illumination every 30 seconds over a 2-minute duration. Scale bars represent 10 microns.

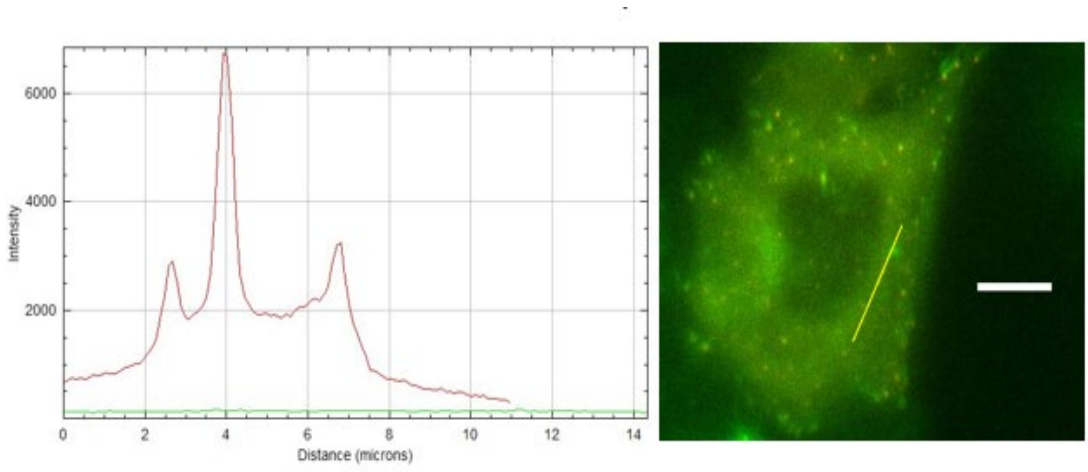

Figure 3.15 Low correlation image analysis of fluorescence intensity colocalization of L209E. This analysis was performed on a selected region containing a group Optoprofilin clusters at the edge of the cell where nonstress condition showed L209E-VASP localization. While the image is depicted in the overlay channel for visual clarity, it represents a composite of multiple channels. The left image demonstrates the overlapping fluorescence intensity of GFP and mCherry, yielding a Pearson's correlation coefficient of 0.76. Right Image shows the portion selected for the test outlined in a box.

To investigate the function of specific profilin residues in the optogenetic system's localization to focal adhesions under non-stress conditions and its clustering response to stress, mutations L123A and H134A were generated within the profilin domain. To assess the expression of these constructs in cells, Western blot analysis was conducted. This aimed to determine any alterations in expression levels of the modified profilin compared to the wild type **(Figure 3.16).** Low expression levels observed for L123A and H134A may indicate suboptimal protein expression and potential competition with endogenous VASP.

Taking a closer look at the position of the two proteins and binding in the Alpha fold 3D model this allowed the ability to identify what residues were interacting with each other and the solvent around **(Figure 3.17).** L1234 is positioned in a hydrophobic residue pocket that is surrounded by rich hydrogen bonding. Solvent stability was important to the environment for many reasons due to the binding reaction rate being affected or a destabilized structure with loss of function when cell environments were altered. Alpha fold for this identified that the water molecules surrounding this residue helped hold the structure in place (Bank, 2025). When observed under the microscope and blue light activation under PBS conditions we saw no recruitment to focal adhesions and when we added the stress solution and did imaging, we did get a cluster response that is typical of OptoProfilin **(Figure 3.18).** This change was not enough to allow localization, but we did get oligomerization from the monomers to form condensates with the endogenous VASP that is within the cell already.

Mutation H134A, located in an exposed region externally to the alpha helix, engages with proline within the VASP domain. This mutation induces alterations in both inter- and intra-structural stability, specifically impacting a tyrosine residue and its surrounding solvent. The two nitrogens on the histidine ring each do a different stability function. One of the nitrogen’s is

bonded to a tyrosine ring on the profilin to keep the hold. The H134A mutation, situated in a surface-exposed region beyond the confines of the alpha helix, directly interacts with a proline residue present within the VASP domain. This specific amino acid substitution triggers notable shifts in both the internal and overall structural stability of the protein. Notably, these alterations significantly influence a particular tyrosine residue and its immediate solvation environment. Within the histidine ring at position 134, the two nitrogen atoms fulfill distinct roles in maintaining stability **(Figure 3.19)**. One of these nitrogen atoms forms a crucial bond with a tyrosine ring located on the profilin molecule, a key interaction responsible for maintaining a stable complex between the two proteins. From this I have pulled together a table of results from the previous experiments showcasing the effects of these mutants **(Table 3.2).** The intensity of one channel is first assessed and then cross-compared to the second channel using the Coloc 2 plugin in FIJI (ImageJ). Once this is completed, the algorithm performs a Pearson's correlation coefficient (PCC) analysis to evaluate the degree of co-localization between the two channels. The PCC value is calculated based on pixel intensity overlap and ranges from -1 to +1, where +1 indicates perfect correlation, 0 indicates no correlation, and values below 0 suggest inverse correlation. Values above 0.5 are considered moderate and strong are above 0.8 with correlation likely. Y39A was weakly correlated while other mutants were moderate to strong.

Table 3.2: **Results from Chapter 3**

Name of VASP Mutant	**Condition**	**Phenotype Observed**	**Correlation Value**	**Correlation Likely?**
Y39A	Stress	None	0.25	No
	PBS	None	0.15	No
P120E	Stress	Condensate	.85	Yes
	PBS	Focal Adhesions	.85	Yes
L209E	Stress	None	.76	Yes
	PBS	Focal Adhesion	.82	Yes
Name of Profilin Mutants				
H134A	Stress	Does not Recruit	N/A	N/A
	PBS	Does not Recruit	N/A	N/A
L123A	Stress	Does Recruit	N/A	N/A
	PBS	Does Recruit	N/A	N/A

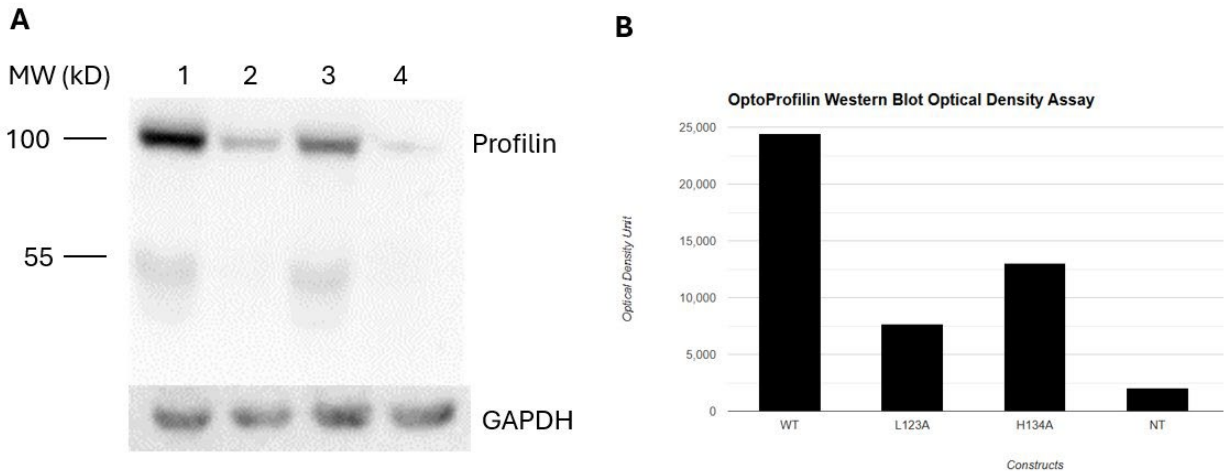

Figure 3.16: **Western blot analysis of the OptoProfilin (Cry2.mCh.Profilin) constructs.** A. Western blot lanes of constructs as followed Lane 1(WT), Lane 2 (L123A), Lane 3 (H134A), Lane 4 (NT). GAPDH was used as loading control. ~103 kDa sized Profilin mutants are shown. B. Optical density assay was performed using ImageJ. OptoProfilin density was normalized to the GAPDH loading control. 20µL of samples loaded in each well.

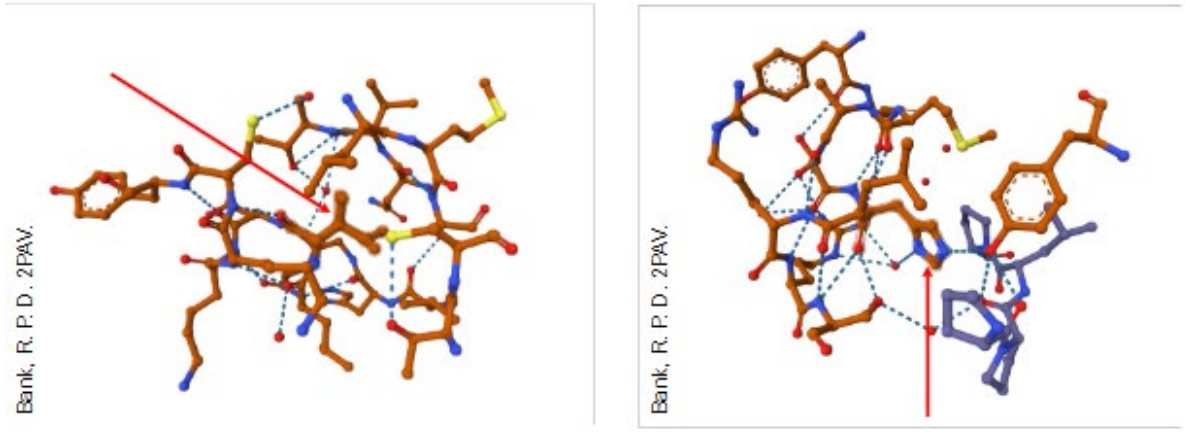

Figure 3.17 Stick figure diagram from AlphaFold of mutation locations. This Depicts the location of L1234 within a hydrophobic pocket stabilized by extensive hydrogen bonds (left). In contrast, H134 is located outside the alpha helix, where it interacts with a proline residue in the VASP domain (right). This mutation affects both the protein's internal and overall stability, specifically influencing a tyrosine residue and its surrounding solvent environment. Image used under Creative Commons license: CC BY- 4.0 DEED.

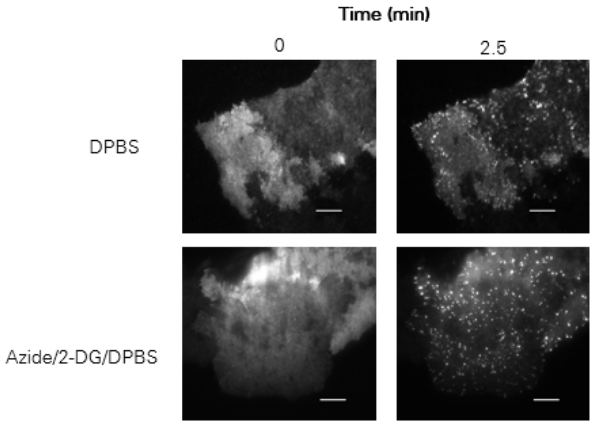

Figure 3.18: L-123 OptoProfilin mutation imaged under non-stress and stress conditions OptoProfilin.mCherry.L123A in PBS is imaged at time 0 minute and 2.5 minutes with blue light activation in the light-activated localization. Time 2.5 min shows recruitment to focal adhesions. Shown at the bottom panel is OptoProfilin.mCherry.L123A after 2.5 min of blue light activation in the light-activated localization under energetic stress conditions (6 mM 2-DG and 10 mM NaN3 in 1X Dulbecco's PBS with Ca2+ and Mg2+). Imaging protocol: 553 nm (50 ms exposure) and 470 nm (50 ms exposure) pulsed illumination every 30 seconds over a 2.5 minute duration. Scale bars represent 10 microns.

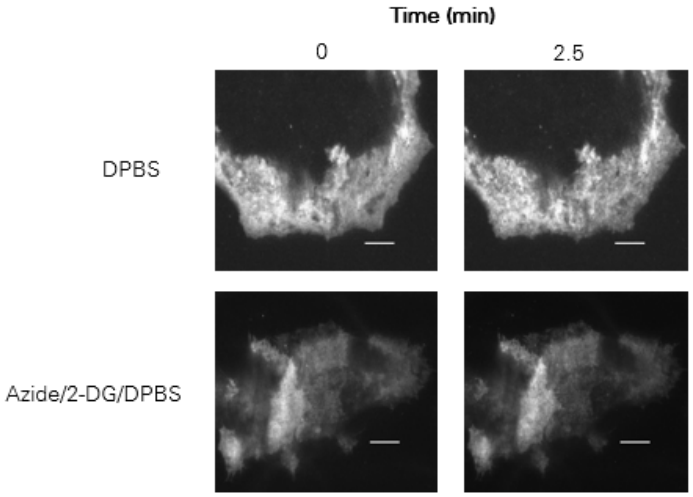

Figure 3.19: H-134 OptoProfilin mutation imaged under non-stress and stress conditions. OptoProfilin.mCherry.H134A in PBS is imaged at time 0 minute and 2.5 minutes with blue light activation with absence of light-activated localization. Time 2.5 min shows no apparent recruitment to focal adhesions. Shown at the bottom panel is OptoProfilin.mCherry.H134A after 2.5 min of blue light activation under energetic stress conditions (6 mM 2-DG and 10 mM NaN3 in 1X Dulbecco's PBS with Ca2+ and Mg2+). Imaging protocol: 553 nm (50 ms exposure) and 470 nm (50 ms exposure) pulsed illumination every 30 seconds over a 2.5 minute duration. Scale bars represent 10 microns.

3.3 Methods and Materials

Cell lines and Transfection

Cell lines and transfection Miniprep quantities of DNA of each construct were created from E. coli and collected for cell transfection. Transfection of HeLa cells was then performed with Calfectin reagent (SignaGen) following manufacturer's suggested protocols. Briefly, for dual transfections in 35 mm glass bottom dishes, plasmid DNA was combined in a 1:1 ratio (1,250 ng per plasmid for dual transfections) in 100 µl of DMEM, followed by the addition of 3 µl of Calfectin reagent. The solution was allowed to incubate at room temperature for 10 min, followed by dropwise addition to cell culture. Transfection solutions were allowed to remain on cells overnight. Cells were maintained at 37°C and 5% CO2 in a humidified tissue culture incubator, in culture medium consisting of DMEM supplemented with 10% FBS and 1% Penicillin-Streptomycin

Fixed cell experiments

Transfected HeLa cells were washed with Dulbecco's PBS (with calcium and magnesium; 3 x 1 mL), prior to treatment with ATP depletion medium (6 mM D-Deoxyglucose and 10 mM Sodium Azide in Dulbecco's PBS) for the indicated time intervals. ATP depletion medium was removed by aspiration, cells washed gently (1X with 1 mL Dulbecco's PBS), then fixed for 45 min with pre-warmed 4% Paraformaldehyde solution (37^{o}C; prepared from 16% PFA (Electron Microscopy Sciences and DPBS) at room temperature for 45 min. Following fixation, cells were washed with PBS, then permeabilized for 3 min using pre-chilled methanol (-20oC). Methanol was removed by aspiration, then cells were blocked for 30 min with an antibody dilution buffer (30 µl Triton X-100, 0.1 g of BSA, 10 mL of Dulbecco's PBS). Cells

then were incubated overnight at 4ºC with primary antibody (anti-Actin (Santa Cruz); 1:500 in antibody dilution buffer). The following day, primary antibody solution was removed by pipette, and cells were washed three times with Dulbecco's PBS. Cells were incubated with Alexa 488 conjugated goat anti-mouse secondary (Invitrogen; 1:200 in antibody dilution buffer) for 1 hour at room temperature, followed by a Dulbecco's PBS wash (1 mL; 3 x 5 min). Cells were stored in Dulbecco's PBS before imaging.

Lipid Spot Protocol

HeLa cells were cultured in Eagle DMEM until they reached 70-80% confluency. Cells were transfected with OptoProfilin construct using a suitable transfection method mentioned above (e.g. Lipofectamine). After transfection, the cells will be incubated with Lipid Spot Dye (Biotium) following the manufacturer's instructions was diluted to a 1X working concentration in cell culture. OptoProfilin was activated in the transfected cells by light illumination. Exposure times were set at 150 ms (GFP, 470 42 nm) and 300 ms (mCherry, 550 nm), with LED light sources at 50% power, and images acquired every 30 seconds over a 10 min time course.

Imaging

Confocal Microscopy: Confocal images of fixed cells were obtained with Olympus IX2-DSU tandem spinning disk confocal laser scanning microscope or with a Zeiss LSM 880 microscope with Airyscan technology. Fluorescence images were colorized and overlaid using FIJI software.

Widefield Microscopy: A Leica DMi8 Live Cell Imaging System, equipped with an OKOLab stage-top live cell incubation system, LASX software, Leica HCX PL APO 63x/1.40-

0.60na oil objective, Lumencor LED light engine, CTRadvanced+ power supply, and a Leica DFC900 GT camera, was used to acquire images. Exposure times were set at 150 ms (GFP, 470 42 nm) and 300 ms (mCherry, 550 nm), with LED light sources at 50% power, and images acquired every 30 seconds over a 10 min time course.

Western blotting

HeLa cells were lysed post-transfection with 200 µL of M-PER lysis buffer (Thermo Scientific) plus protease inhibitors. After 10 min on a rotary shaker at room temperature, lysates were collected and centrifuged for 15 min (94 rcf; 4˚C). Supernatants were used for further experiments. The resulting lysates were subjected to electrophoresis on a 10% SDS-PAGE gel and then transferred onto PVDF membranes (20 V, overnight, at 4 ˚C). Membranes were then blocked for 1 h with 5% BSA in TBS with 1% Tween (TBST), followed by incubation with primary antibody (Anti-mCherry antibody (Cell Signaling #43590); 1:1000 dilution in 5% BSA – TBST; Anti-GFP antibody (Santa Cruz #sc-8334); 1:1000 dilution in 5% BSA – TBST) overnight at 4 °C on a platform rocker. The membranes were then washed 3 x 5 min each with TBST and incubated with the appropriate secondary antibody in 5% BSA – TBST for 2 hours at room temp. After washing 3 x 5 min with TBST, the membranes were exposed to a chemiluminescent substrate for 5 min and imaged using an Azure cSeries imaging station.

Statistical analysis

Plots were constructed using FIJI equipped with Coloc 2 Add-on (Schindelin et al., 2019). Based on calculating the "spatial resolution of the microscope and the "point spread function (PSF) of the fluorescent signals to determine how many pixels a single fluorescent spot

occupies. Each channel was used to analyze a region of interest, and a constant is set for the intensity of pixels at the time of the test. The intensity of one channel is assessed and then cross-compared to the second channel. Once this is completed, a Pearson's correlation is performed by the algorithm. Two-channel images were assessed by specific regions of interest that were selected using the line tool to isolate the relevant biological area for analysis. the Coloc 2 plugin was launched and the ROI was chosen from the channel, with the Point Spread Function (PSF) size activated. Analysis and interpretation of the correlation coefficients and scatterplots from the results window were interpreted and provided.

References

Ball, L. J.; Jarchau, T.; Oschkinat, H.; Walter, U. EVH1 Domains: Structure, Function and Interactions. FEBS Letters 2001, 513(1), 45–52. https://doi.org/10.1016/s0014-5793(01)03291-4.

Banani, S. F.; Lee, H. O.; Hyman, A. A.; Rosen, M. K. Biomolecular Condensates: Organizers of Cellular Biochemistry. Nature Reviews Molecular Cell Biology 2017, 18(5), 285–298. https://doi.org/10.1038/nrm.2017.7.

Bansal, A.; Shikha, S.; Zhang, Y. Towards Translational Optogenetics. Nature Biomedical Engineering 2022, 7. https://doi.org/10.1038/s41551-021-00829-3.

Basu, S.; Kustanovich, I.; Lamprecht, R. Arp2/3 and VASP Are Essential for Fear Memory Formation in Lateral Amygdala. eneuro 2016, 3(6), ENEURO.0302-16.2016. https://doi.org/10.1523/eneuro.0302-16.2016.

Blanchoin, L.; Boujemaa-Paterski, R.; Sykes, C.; Plastino, J. Actin dynamics, architecture, and mechanics in cell motility. Physiological Reviews 2014, 94(1), 235–263. https://doi.org/10.1152/physrev.00018.2013.

Borovac, J. A.; D'Amico, E.; Nowak, K. J.; Laing, N. G.; Ravine, D.; Anderton, R. S. Profilin 1 in protein aggregation and neurodegenerative diseases. Cellular and Molecular Life Sciences 2018, 75(17), 3107–3118. https://doi.org/10.1007/s00018-018-2837-8.

Brumbaugh-Reed, E.H., Gao, Y., Aoki, K. et al. Rapid and reversible dissolution of biomolecular condensates using light-controlled recruitment of a solubility tag. Nat Commun 15, 6717 (2024). https://doi.org/10.1038/s41467-024-50858-0

Bunner, W. D.; Freeman, R. S.; Hughes, R. M. The CofActor Optogenetic System for Light- and Stress-Gated Control of Cofilin-Actin Interactions and Cytoskeletal Anomalies. ACS Synthetic Biology 2021, 10(10), 2693–2707. https://doi.org/10.1021/acssynbio.1c00278.

Che, D. L.; Duan, L.; Zhang, K.; Cui, B. The Dual Characteristics of Light-Induced Cryptochrome 2, Homo-Oligomerization and Heterodimerization, for Optogenetic Manipulation in Mammalian Cells. ACS synthetic biology 2015, 4(10), 1124–1135. https://doi.org/10.1021/acssynbio.5b00048.

Christie, J. M. Phototropin Blue-Light Receptors. Annual Review of Plant Biology 2007, 58(1), 21–45. https://doi.org/10.1146/annurev.arplant.58.032806.103951.

Cuevas-Velazquez, C. L.; Vellosillo, T.; Guadalupe, K.; Hermann Broder Schmidt; Yu, F.; Moses, D.; Brophy, J. A. N.; Cosio-Acosta, D.; Das, A.; Wang, L.; Jones, A. M.; Covarrubias, A. A.; Sukenik, S.; Dinneny, J. R. Intrinsically Disordered Protein

Biosensor Tracks the Physical-Chemical Effects of Osmotic Stress on Cells. Nature Communications 2021, 12(1). https://doi.org/10.1038/s41467-021-25736-8.

Döppler, H.; Storz, P. Regulation of VASP by Phosphorylation. Cell Adhesion & Migration 2013, 7(6), 492–496. https://doi.org/10.4161/cam.27351.

Emiliani, V.; Entcheva, E.; Hedrich, R.; Hegemann, P.; Konrad, K. R.; Lüscher, C.; Mahn, M.; Pan, Z.-H.; Sims, R. R.; Vierock, J.; Yizhar, O. Optogenetics for Light Control of Biological Systems. Nature Reviews Methods Primers 2022, 2(1). https://doi.org/10.1038/s43586-022-00136-4.

Figley, M. D.; Bieri, G.; Kolaitis, R. M.; Taylor, J. P.; Gitler, A. D. Profilin 1 associates with stress granules and ALS-linked mutations alter stress granule dynamics. Journal of Neuroscience 2014, 34(24), 8083–8097. https://doi.org/10.1523/JNEUROSCI.0542-14.2014.

Gau, D.; Veon, W.; Shroff, S. G.; Roy, P. The VASP–Profilin1 (Pfn1) Interaction Is Critical for Efficient Cell Migration and Is Regulated by Cell–Substrate Adhesion in a PKA-Dependent Manner. Journal of Biological Chemistry 2019, 294(17), 6972–6985. https://doi.org/10.1074/jbc.ra118.005255.

Gutsche-Perelroizen, Irina, and Jean Lepault. Filament Assembly from Profilin-Actin - Sciencedirect, www.sciencedirect.com/science/article/pii/S0021925819875798. Accessed 17 July 2025.

Hernández-Candia, C.N., Pearce, S. & Tucker, C.L. A modular tool to query and inducibly disrupt biomolecular condensates. Nat Commun 12, 1809 (2021). https://doi.org/10.1038/s41467-021-22096-1

Hildebrand, J. D.; Schaller, M. D.; Parsons, J. T. Paxillin, a Tyrosine Phosphorylated Focal Adhesion-Associated Protein Binds to the Carboxyl Terminal Domain of Focal Adhesion Kinase. Molecular Biology of the Cell 1995, 6(6), 637–647. https://doi.org/10.1091/mbc.6.6.637.

Hoffelner, B. S.; Andreev, S.; Plank, N.; Koch, P. Photocaging of Pyridinylimidazole-Based Covalent JNK3 Inhibitors Affords Spatiotemporal Control of the Binding Affinity in Live Cells. Pharmaceuticals 2023, 16(2), 264–264. https://doi.org/10.3390/ph16020264.

Hososhima, S.; Sakai, N.; Yawo, H. Molecular insights of a next-generation channelrhodopsin, ChRmine. Scientific Reports 2023, 13(1), 4649. https://doi.org/10.1038/s41598-023-31807-7.

Kanchanawong, P.; Shtengel, G.; Pasapera, A. M.; Ramko, E. B.; Davidson, M. W.; Hess, H. F.; Waterman, C. M. Nanoscale Architecture of Integrin-Based Cell Adhesions. Nature 2010, 468(7323), 580–584. https://doi.org/10.1038/nature09621.

Lee, M.; Moon, H. C.; Jeong, H.; Dong Wook Kim; Hye Yoon Park; Shin, Y. Optogenetic Control of MRNA Condensation Reveals an Intimate Link between Condensate Material Properties and Functions. Nature Communications 2024, 15(1). https://doi.org/10.1038/s41467-024-47442-x.

Legerstee, K.; Geverts, B.; Slotman, J. A.; Houtsmuller, A. B. Dynamics and Distribution of Paxillin, Vinculin, Zyxin and VASP Depend on Focal Adhesion Location and Orientation. Scientific Reports 2019, 9(1). https://doi.org/10.1038/s41598-019-46905-2.

Legerstee, K.; Houtsmuller, A. A Layered View on Focal Adhesions. Biology 2021, 10(11), 1189. https://doi.org/10.3390/biology10111189.

Litschel, T.; Kelley, C. F.; Cheng, X.; Babl, L.; Mizuno, N.; Case, L. B.; Schwille, P. Membrane-Induced 2D Phase Separation of the Focal Adhesion Protein Talin. Nature Communications 2024, 15(1). https://doi.org/10.1038/s41467-024-49222-z.

Mahboubi, H.; Stochaj, U. Profilins in the Nucleus: A Journey from the Cytoskeleton into the Cell Interior. Cells 2017, 6(1), 5. https://doi.org/10.3390/cells6010005.

Mann, N.; Hill, J. T.; Wang, K.; Hughes, R. OptoProfilin: A Single Component Biosensor of Applied Cellular Stress. ChemBioChem 2024, 25(9). https://doi.org/10.1002/cbic.202400007.

Marnik, E. A.; Updike, D. L. Membraneless Organelles: P Granules in Caenorhabditis Elegans. Traffic 2019, 20(6), 373–379. https://doi.org/10.1111/tra.12644.

Martin, M.; Ahern-Djamali, S. M.; Hoffmann, F. M.; Saxton, W. M. Abl Tyrosine Kinase and Its Substrate Ena/VASP Have Functional Interactions with Kinesin-1. Molecular Biology of the Cell 2005, 16(9), 4225–4230. https://doi.org/10.1091/mbc.E05-02-0116.

Michelot, A.; Guérin, C.; Huang, S.; Ingouff, M.; Richard, S.; Van Damme, D.; Traas, J.; Blanchoin, L.; Staiger, C. J. The formin homology 1 domain of Arabidopsis FORMIN1 is essential for actin nucleation and polymerization in vitro. The Plant Cell 2005, 17(7), 2230–2246. https://doi.org/10.1105/tpc.105.032653.

Mouneimne G, Hansen SD, Selfors LM, Petrak L, Hickey MM, Gallegos LL, Simpson KJ, Lim J, Gertler FB, Hartwig JH, Mullins RD, Brugge JS. Differential remodeling of actin cytoskeleton architecture by profilin isoforms leads to distinct effects on cell migration and invasion. Cancer Cell. 2012 Nov 13;22(5):615-30. doi: 10.1016/j.ccr.2012.09.027. PMID: 23153535; PMCID: PMC3500527.

Munsie, L. N.; Truant, R. The role of cofilin-actin rods in neurodegeneration and cellular stress. Cellular and Molecular Life Sciences 2012, 69(20), 3373–3387. https://doi.org/10.1007/s00018-012-0986-0.

Oldenburg, J.; van der Krogt, G.; Twiss, F.; Bongaarts, A.; Habani, Y.; Slotman, J. A.; Houtsmuller, A.; Huveneers, S.; de Rooij, J. VASP, Zyxin and TES Are Tension-Dependent Members of Focal Adherens Junctions Independent of the α-Catenin-Vinculin Module. Scientific Reports 2015, 5(1). https://doi.org/10.1038/srep17225.

Pantaloni, D.; Carlier, M. F. How profilin promotes actin filament assembly in the presence of thymosin beta 4. Cell 1993, 75(5), 1007–1014. https://doi.org/10.1016/0092-8674(93)90520-j.

Pollard, T. D.; Cooper, J. A. Quantitative analysis of the effect of Acanthamoeba profilin on actin filament nucleation and elongation. Biochemistry 1984, 23(26), 6631–6641. https://doi.org/10.1021/bi00321a039.

Read, D.; O'Leary, C.; Crudele, J. M.; Fochler, S.; Ravits, J.; Taylor, J. P.; Gitcho, M. A. Profilin 1 (PFN1) mutations cause ALS/FTD by disrupting cortical neuronal function. Acta Neuropathologica Communications 2023, 11(1), 12. https://doi.org/10.1186/s40478-023-01507-6.

Rein, B.; Deussing, J. M. Optogenetics in psychiatric research: the VTA as a model. Molecular Psychiatry 2012, 17(11), 1066–1074. https://doi.org/10.1038/mp.2012.82.

Reinhard, M.; Giehl, K.; Abel, K.; Haffner, C.; Jarchau, T.; Hoppe, V.; Jockusch, B. M.; Walter, U. The Proline-Rich Focal Adhesion and Microfilament Protein VASP Is a Ligand for Profilins. The EMBO Journal 1995, 14(8), 1583–1589. https://doi.org/10.1002/j.1460-2075.1995.tb07146.x.

Reinhard, M.; Jouvenal, K.; Tripier, D.; Walter, U. Identification, Purification, and Characterization of a Zyxin-Related Protein That Binds the Focal Adhesion and Microfilament Protein VASP (Vasodilator-Stimulated Phosphoprotein). Proceedings of the National Academy of Sciences 1995, 92(17), 7956–7960. https://doi.org/10.1073/pnas.92.17.7956.

Rotty, J. D.; Wu, C.; Haynes, E. M.; Suarez, C.; Winkelman, J. D.; Johnson, H. E.; Haugh, J. M.; Kovar, D. R.; Bear, J. E. Profilin-1 serves as a gatekeeper for actin assembly by Arp2/3-dependent and -independent pathways. Developmental Cell 2015, 32(1), 54–67. https://doi.org/10.1016/j.devcel.2014.10.026.

Schindelin, J., Arganda-Carreras, I., Frise, E., Kaynig, V., Longair, M., Pietzsch, T., … Cardona, A. (2012). Fiji: an open-source platform for biological-image analysis. Nature Methods, 9(7), 676–682. doi:10.1038/nmeth.2019

Suarez, C.; Carroll, R. T.; Burke, T. A.; Christensen, J. R.; Bestul, A. J.; Sees, J. A.; James, A. L.; Sirotkin, V.; Kovar, D. R. Profilin regulates F-actin network homeostasis by favoring formin over Arp2/3 complex. Developmental Cell 2015, 32(1), 43–53. https://doi.org/10.1016/j.devcel.2014.10.020.

Tachibana H, Minoura K, Omachi T, Nagao K, Ichikawa T, Kimura Y, Kono N, Shimanaka Y, Arai H, Ueda K, Kioka N. The plasma membrane of focal adhesions has a high content of cholesterol and phosphatidylcholine with saturated acyl chains. J Cell Sci. 2023 Aug 15;136(16):jcs260763. doi: 10.1242/jcs.260763. Epub 2023 Aug 17. PMID: 37470177.

Tiwari, P.; Tolwinski, N. S. Using Optogenetics to Model Cellular Effects of Alzheimer's Disease. International Journal of Molecular Sciences 2023, 24(5), 4300. https://doi.org/10.3390/ijms24054300.

Turner, C. E. Paxillin and Focal Adhesion Signalling. Nature Cell Biology 2000, 2(12), E231–E236. https://doi.org/10.1038/35046659.

UniProt. Uniprot.org. https://www.uniprot.org/uniprotkb/P50552/entry (accessed 2024-08-05).

Walter, A.; Tissir, F.; Wuytack, F.; Heir R., K.; Prakash, N.; Storkebaum, E. Cofilin/Twinstar-Actin Rods in Axonal Degeneration: A Mini-Review. Frontiers in Molecular Neuroscience 2021, 14, 762931. https://doi.org/10.3389/fnmol.2021.762931.

Wang, Q.; Lin, C. A Structural View of Plant CRY2 Photoactivation and Inactivation. Nature structural & molecular biology 2020, 27(5), 401–403. https://doi.org/10.1038/s41594-020-0432-6.

Wang, R.; Liao, G.; Wang, Y.; Tang, D. D. Distinctive Roles of Abi1 in Regulating Actin-Associated Proteins during Human Smooth Muscle Cell Migration. Scientific Reports 2020, 10(1). https://doi.org/10.1038/s41598-020-67781-1.

Wang, Z.; Wu, L.; Cheng, X.; Lin, X.; Ying, Z.; Wu, S. The Emerging Role of Profilin-1 in Cardiovascular Diseases. Journal of Cardiovascular Development and Disease 2022, 9(9), 286. https://doi.org/10.3390/jcdd9090286.

Wurz, A. I.; Bunner, W.; Erzsebet Szatmari; Hughes, R. M. CRY–BARs: Versatile Light-Gated Molecular Tools for the Remodeling of Membrane Architectures. Journal of Biological Chemistry 2022, 298(10), 102388–102388. https://doi.org/10.1016/j.jbc.2022.102388.

Yoshigi, M.; Hoffman, L. M.; Jensen, C. C.; Yost, H. J.; Beckerle, M. C. Mechanical Force Mobilizes Zyxin from Focal Adhesions to Actin Filaments and Regulates Cytoskeletal Reinforcement. Journal of Cell Biology 2005, 171(2), 209–215. https://doi.org/10.1083/jcb.200505018.

Zhu J, Ma Y, Xu J, Li Y, Wan P, Qi Y, Yu T, Zhu D. Dec-DISCO: decolorization DISCO clearing for seeing through the biological architectures of heme-rich organs. Biomed Opt Express. 2021 Aug 11;12(9):5499-5513. doi: 10.1364/BOE.431397. PMID: 34692197; PMCID: PMC8515970.